

Time-varying drainage basin development and erosion on volcanic edifices

Daniel O'Hara^{1,2}, Liran Goren³, Roos M.J. van Wees¹, Benjamin Campforts⁴, Pablo Grosse^{5,6}, Pierre Lahitte⁷, Gabor Kereszturi⁸, Matthieu Kervyn¹

¹Department of Geography, Vrije Universiteit Brussel, Pleinlaan 2, 1050 Elsene.

²Helmholtz Center Potsdam, GFZ German Research Center for Geosciences, Potsdam, Germany.

³Ben Gurion University of the Negev, Department of Earth and Environmental Sciences, Beer-Sheva, Israel

⁴Institute of Arctic and Alpine Research, University of Colorado Boulder, Boulder, CO, USA

⁵Consejo Nacional de Investigaciones Científicas y Técnicas (CONICET), Argentina

⁶Fundación Miguel Lillo, Miguel Lillo 251, (4000) Tucumán, Argentina

⁷Université Paris-Saclay, CNRS, Laboratoire GEOPS, Rue du Belvédère, 91405 Orsay, France

⁸Volcanic Risk Solutions, School of Agriculture and Environment, Massey University, 4474, New Zealand

Correspondence to: Daniel O'Hara (Daniel.OHara@vub.be)

Abstract. The erosional state of a landscape is often assessed through a series of metrics that quantify the morphology of drainage basins and divides. Such metrics have been well-explored in tectonically-active environments to evaluate the role of different processes in sculpting topography, yet relatively few works have applied these analyses to radial landforms such as volcanoes. We quantify drainage basin geometries on volcanic edifices of varying ages using common metrics (e.g., Hack's Law, drainage density, number of basins that reach the edifice summit, as well as basin hypsometry integral, length, width, relief, and average topographic slope). Relating these measurements to the log-mean age of activity for each edifice, we find that drainage density, basin hypsometry, basin length, and basin width quantify the degree of erosional maturity for these landforms. We also explore edifice drainage basin growth and competition by conducting a divide mobility analysis on the volcanoes, finding that young volcanoes are characterized by nearly-uniform fluvial basins within unstable configurations that are more prone to divide migration. As basins on young volcanoes erode, they become less uniform but adapt to a more stable configuration with less divide migration. Finally, we analyze basin spatial geometries and outlet spacing on edifices, discovering an evolution in radial basin configurations that differ from typical linear mountain ranges. From these, we present a novel conceptual model for edifice degradation that allows new interpretations of composite volcano histories and provides predictive quantities for edifice morphologic evolution.

1.0 Introduction

Understanding how drainage basins on eroding landforms develop and evolve is a fundamental principle of Geomorphology. Over regional scales, basin geometry, structure, and spacing evolve in response to both external (e.g., climate, tectonics; Castelltort et al., 2012; Duvall and Tucker, 2015; Han et al., 2015; Yang et al., 2015) and internal (e.g., channel piracy; Bishop, 1995; Whipple et al., 2016) forcing as topographic slopes adjust to develop and maintain an equilibrium between erosion and uplift (e.g., Willett et al., 2001; Castelltort et al., 2009). As these landscapes adjust, transient signals within basins propagate upstream to surrounding channel heads, where opposing signals between adjacent basins drive divide migration that modify available area for overland flow (e.g., Willett et al., 2014; O'Hara et al., 2019).

Work in the 20th century established foundational relationships between basin drainage areas, lengths, and slopes (e.g., Horton, 1945; Strahler, 1952; Hack, 1957; Flint, 1974), providing the basis for analyzing landscape disequilibrium and evolution in both tectonically-active (e.g., Kirby and Whipple, 2012; Fox et al., 2014) and passive (Prince and Spotila, 2013; Willett et al., 2014; Braun, 2018) regions. These relationships are built on the

Deleted: Goren²

Formatted: Superscript

Deleted: Grosse^{4,5}

Deleted: Campforts³

Deleted: Lahitte⁶

Deleted: Kereszturi⁷

Deleted: ²

Deleted: ³

Deleted: ⁴

Deleted: ⁵

Deleted: ⁶

Deleted: ⁷

Deleted: basin geometries in

Deleted: Castelltort et al., 2012; Duvall and Tucker, 2015; Han et al., 2015; Yang et al., 2015

Deleted: (e.g., Willett et al., 2014; O'Hara et al., 2019)

Deleted: (e.g., Kirby and Whipple, 2012; Fox et al., 2014)

Deleted: regions

Deleted: .

60 assumption of a dominantly-dendritic fluvial network existing on a near-linear primary landform (e.g., a mountain
61 range; Castelltort and Simpson, 2006). Furthermore, basin competition is often considered in the simplified
62 configuration of a binary drainage system, where a divide supports only two opposing basins that compete across it
63 (e.g., Gilbert, 1909; Mudd and Furbish, 2007).

64 Although dendritic channel networks are most prevalent on Earth, they are not the only type of configuration.
65 Trellis, rectangular, parallel, and radial drainages also occur (Howard, 1967). The formation of these other drainages
66 often relate to the region's tectonic, volcanic, or glacial history, subsurface structure, or geometry of the primary
67 landform that they erode (Zernitz, 1932). However, compared to dendritic basins, studies that explore the geometries
68 and evolution of other drainage settings are scarce (e.g., Mejía and Niemann, 2008; Becerril et al., 2021; Hamawi et
69 al., 2022).

70 Volcanic edifices are characterized by radial drainages. In these settings, quantifying drainage evolution can be
71 challenging as these landforms experience interspersed, short-term eruptive episodes superimposed onto the long-
72 term degradation record (e.g., Thouret et al., 2014). These stochastic volcanic events often produce spatially-varying
73 excess sediment supply in the form of pyroclasts with varying grain properties that significantly alter fluvial
74 transport on decadal scales (e.g., Major et al., 2018; Hayes et al., 2002). Additionally, drainage formation can lag
75 behind surfacing by volcanic deposits over 1 – 100 kyr timescales due to transmission losses associated with
76 permeable volcanic material (e.g., lava flows, pyroclasts; Lohse and Dietrich, 2005; Jefferson et al., 2010; Sweeney
77 and Roering, 2017). Finally, the more symmetric drainage divide configuration typical of linear mountain ranges
78 breaks down on volcanic edifices due to their radial nature, with multiple catchments constrained to the conical
79 structure of the volcano and converging towards one to a few main summits. Despite these challenges, volcanic
80 edifices represent ideal primary landforms to investigate drainage evolution due to their well-defined conical initial
81 conditions, datable surfaces, and scarce inheritance from regional tectonics. Furthermore, quantifying the
82 relationships between edifice construction and drainage basin morphology provides new insight for investigating
83 edifices remotely, and can thus expand our understanding of basin dynamics while also complementing field-based
84 surveys to resolve volcano edifice histories.

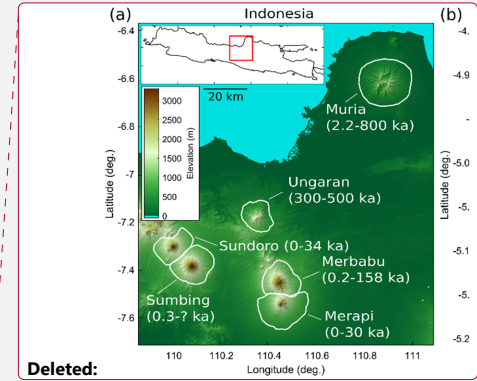
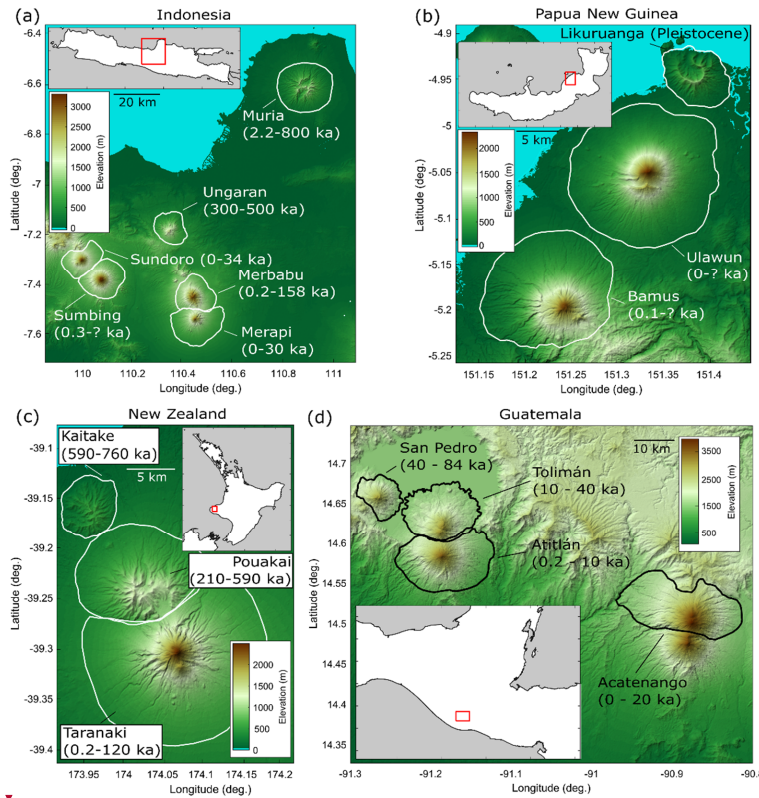
85 Here, we explore the development of drainage basins and topography on stratovolcanoes from Indonesia, Papua
86 New Guinea, New Zealand, and Guatemala (Fig. 1). Using common hydrographic metrics and broad volcanic
87 histories, we determine stages of maturation during basin evolution and derive a new generalized model for
88 stratovolcano degradation that builds off of previous studies (Ollier, 1988). We then quantify divide mobility on
89 radial structures within the context of our conceptual model and discuss the applicability of our analyses to
90 characterize an edifice's history.

Field Code Changed

Deleted: Volcanic edifices are characterized by radial drainages. In these settings, quantifying drainage evolution can be challenging as these landforms experience interspersed, short-term eruptive episodes superimposed onto the long-term degradation record (e.g., Thouret et al., 2014). Additionally, drainage formation can lag behind surfacing by volcanic deposits over 1 – 100 kyr timescales due to transmission losses associated with permeable volcanic material (e.g., lava flows, pyroclasts; Lohse and Dietrich, 2005; Jefferson et al., 2010; Sweeney and Roering, 2017). Finally, the binary drainage divide typical of linear mountain ranges breaks down on volcanic edifices due to their radial nature, with multiple catchments constrained to the conical structure of the volcano and converging towards a single main summit. Despite these challenges, volcanic edifices represent ideal primary landforms to investigate drainage evolution due to their well-defined conical initial conditions, datable surfaces, and scarce inheritance from regional tectonics. Furthermore, quantifying the relationships between edifice construction and drainage basin morphology provides new insight for investigating edifices remotely, and can thus expand our understanding of basin dynamics while also complementing field-based surveys to resolve volcano edifice histories.¶

Deleted: and

Deleted: volcanic edifice



Deleted:

117

118 **Figure 1** – Regional maps of 16 analyzed edifices from (a) Indonesia, (b) Papua New Guinea, (c) New Zealand, and (d)
 119 Guatemala. Solid white lines in a-c and solid black lines in d represent edifice boundaries (boundary definition described in
 120 Methods). Text describes volcano names and known ages of activity (Table T2).

121 **2.0 Methods**

122 To constrain the temporal evolution of stratovolcano morphologies, we focus on closely-spaced volcano sets (Fig.
 123 1). The advantages of this approach are that within each respective region, 1) volcanoes were likely fed by similar
 124 magma sources (e.g., Locke and Cassidy, 1997; Haapala et al., 2005; Mulyaningsih and Shaban, 2020), constructed
 125 by similar volcanic deposits, and thus had similar volcanic shapes, 2) edifices experienced similar climate
 126 conditions, 3) volcano sets have radiometric ages related to their initiation and most recent eruption that are
 127 comparable, providing constraints on their overall lifespan, and 4) volcanoes within the same set were active over
 128 different time intervals, thus showing contrasting time-dependent degrees of dismantling within a short (10³'s of km)
 129 distance. In order to consider drainage basin evolution through fluvial erosion from the perspective of radial
 130 landforms, we exclude volcano massifs from our analysis, as well as any volcano with recognizable collapse scars,
 131 and only consider volcanoes that do not have an extensive glacial history. All analyzed volcanoes are classified as
 132 stratovolcanoes by the Smithsonian Global Volcanism Program (Global Volcanism Program, 2013).

Formatted: Font: Not Bold

Deleted: 12

Formatted: Font: Not Bold

Deleted: and

Formatted: Font: Not Bold

Deleted: . White

Formatted: Font: Not Bold

Formatted: Font: Not Bold

Deleted: .

Formatted: Font: Not Bold

Deleted: We focus on closely-spaced sets of volcanic edifices (Fig. 1). Within each respective region, volcano sets are fed by similar magma sources and likely experienced similar climate conditions, but the volcanoes were active over different time intervals and show spatially-varying degrees of degradation. We exclude complex massifs from the analysis and consider only relatively simple edifices.¶

2.1 Edifice Delineation

Although automated algorithms exist to generate volcano edifice boundaries (e.g., Bohnenstiehl et al., 2012; Euillades et al., 2013), these often create conservative limits around the edifice that ignore lower flanks and volcano-sedimentary aprons (e.g., O'Hara et al., 2020). We thus follow the method suggested by van Wees et al. (2021) to delineate edifice boundaries from surrounding topography. Using 30-m Shuttle Radar Topography Mission (SRTM) Digital Elevation Models (DEMs) (Farr et al., 2007), we first generate hillshade, aspect, and local slope rasters of the raw topography. Lower edifice flanks are generally characterized by slope angles greater than some threshold value (Karátson et al., 2012); we therefore remove short-wavelength variations of the slope raster by filtering it over a 300 m wavelength (O'Hara et al., 2020) and contour regions that surpass a 3° slope threshold (van Wees et al., 2021). Using these maps as visual aids, we then hand-draw boundaries that separate the edifice from surrounding terrain. Afterwards, the DEMs are clipped using these boundaries to isolate the edifices for morphometric analysis. The planform areas of edifice boundaries derived using this method range from 30.2 km² (Kaitake, New Zealand) to 432.7 km² (Muria, Indonesia).

2.2 Edifice Basin Morphology

We analyze edifice basin morphologies with DrainageVolc, a series of scripts modified from TopoToolbox (Schwanghart and Scherler, 2014), which is designed to investigate volcanic topography through a set of topography-, drainage-, and channel-based analyses. The metrics considered here are commonly used within tectonic settings but have not previously been applied to radial drainages. Figure 2 displays an example of our methods using Ungaran volcano in Indonesia.

We first fill sinks in the DEM through TopoToolbox's preprocessing algorithm (Schwanghart and Scherler, 2014) to ensure continuous flow to the edifice boundary and extract drainage basins from topography using steepest-descent flow routing (Fig. 2a). We then perform a series of analyses related to basin geometry. The lengths (L) of all basins draining to the edifice boundaries are calculated by determining mid-point paths between basin divides perpendicular to the Euclidean distance between the highest and lowest reaches of the basin, irrespective of whether there is an actual flow channel in this path (Fig. 2d). Assuming basins with total drainage areas (A) greater than some threshold (A_T) support overland flow, we explore the correlation between the lengths and drainage areas of these basins through a power-law regression to derive the Hack's Law relationship (Fig. 2b) for the edifice as (Hack, 1957)

$$L = k_a A^H, \quad (1)$$

where k_a and H are Hack's coefficient and exponent, respectively. H values are compared across edifices as this exponent describes general basin geometry, with values of ~0.47 – 0.6 typically attributed to dendritic systems (Hack, 1957; Mueller, 1972). Our Hack's Law derivation uses basin lengths as opposed to typical flow path lengths to remove the effects of channel sinuosity and focus explicitly on basin geometry; however, within the context of our edifice basins, this derivation does not significantly alter our results, and values are thus comparable to those of previous studies (Fig. S1). We also analyze the density of the edifice's channel network by extracting flow paths

Deleted: We follow the method of

Deleted: Although automated algorithms exist to generate boundaries (e.g., Bohnenstiehl et al., 2012; Euillades et al. [1]

Deleted: angle

Deleted: (Karátson et al., 2012)

Deleted: filter topography using

Deleted: reclassify the slope map using

Deleted: None of the chosen volcanoes have closed s (... [2]

Deleted: the

Moved down [1]: Figure 2 – Analyzed basin metrics.

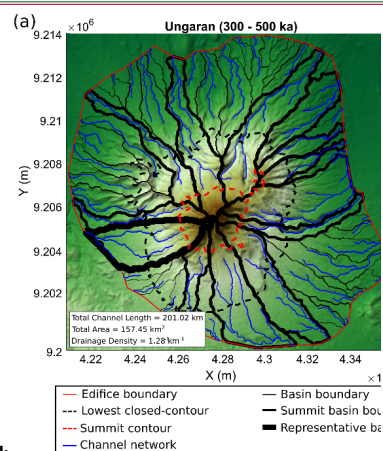
Moved down [3]: c: Scaled edifice metrics. Red line

Formatted: Font: Not Bold

Formatted: Font: Not Bold

Deleted: Gray line represents cross-basin direction (... [5]

Moved down [4]: e: Cross-basin values along basin



Deleted:

Formatted: Font: Not Bold

Deleted: a: Map of Ungaran volcano (Indonesia), (... [3]

Moved down [2]: b: Hack's Law relationship between

Formatted: Font: Not Bold

Deleted: Black circles are basins used in power-law (... [4]

Formatted: Font: Not Bold

Formatted: Font: Not Bold

Deleted: Black line is relief along flowpath, blue lin (... [6]

Deleted: analyzes

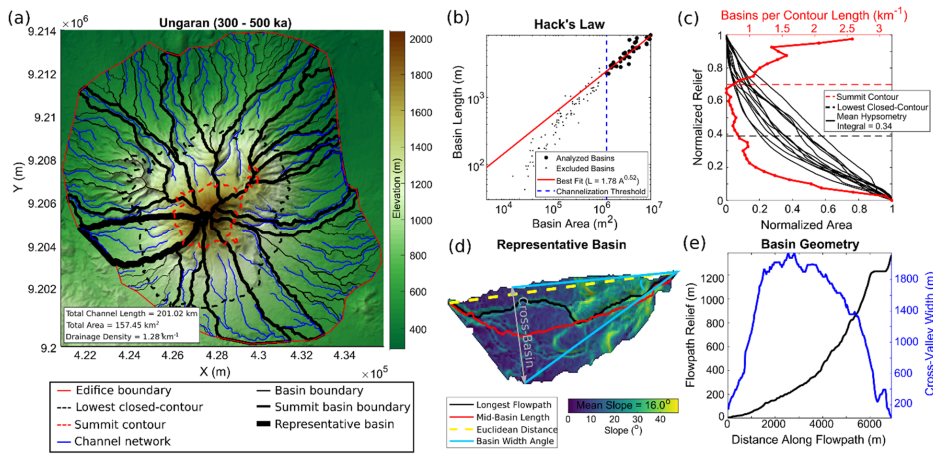
Deleted: then

Deleted: mid-point

229 with drainage areas greater than A_T from the landform, and calculate the edifice-scale drainage density as (Horton,
 230 1945)

$$231 \quad DD = \frac{\sum L_c}{A_E}, \quad (2)$$

232 where $\sum L_c$ is the cumulative sum of all channel lengths and A_E is the planform area of the edifice's boundary (Fig.
 233 2a). Using an automated slope-area analysis of basins to determine the drainage area threshold that best corresponds
 234 with the power-law decrease in slope (Montgomery and Dietrich, 1994) for each edifice (Supplemental text; Fig.
 235 S2), we find A_T ranges between 0.32 – 1.62 km², with a mean threshold of 0.85 km² (Table T1). For consistency
 236 across all edifices, we assume a constant drainage area threshold of 1.0 km² to delineate networks. Sensitivity
 237 analysis (Fig. S3) demonstrates that although the selection of A_T does not significantly impact the general behavior
 238 of drainage density results, the Hack's Law exponent is more sensitive to this choice.



240 **Figure 2 – Analyzed basin metrics.** **a:** Example from the map of Ungaran volcano (Indonesia), colored lines defined in the
 241 legend. **b:** Hack's Law relationship between basin areas and lengths. Black circles are basins used in the power-law analysis,
 242 black dots are excluded basins; blue-dashed line is the drainage area threshold (A_T : 1.0 km²) for channelization. **c:** Scaled edifice
 243 metrics. Red line shows normalized number of basins along elevation contours. Black lines are summit basin hypsometry curves.
 244 **d:** Local slope and geometry values of representative basin (thick black line in 2a). Gray double-arrow represents cross-basin
 245 direction (i.e., the extent of the basin) perpendicular to the Euclidean basin length. **e:** Cross-basin values along basin shown in 2d.
 246 Black line is relief along the flowpath, blue line is cross-valley width.

247 Afterwards, we calculate mean values of basin geometries on each edifice. Rather than analyze the geometry of all
 248 basins that exist on a volcano, we limit our analysis to larger basins that best characterize the edifice's drainage,
 249 and thus its dismantling. These large characteristic basins may be determined using a variety of methods, such as
 250 through an arbitrary number or percentage of basin sizes, using the basins that are within some radial distance of the
 251 edifice's peak, or determining basins that extend to some portion of the edifice's height. Determining characteristic
 252 basins by an arbitrary number or percentage of basin sizes may introduce bias as the population of basins drastically

Deleted: .
 Deleted: 42
 Deleted: 78
 Deleted: Supplemental text
 Deleted: .5

Moved (insertion) [1]
 Formatted: Font: Not Bold
 Moved (insertion) [2]
 Formatted: Font: Not Bold
 Moved (insertion) [3]
 Formatted: Font: Not Bold
 Formatted: Font: Not Bold
 Formatted: Font: Not Bold
 Moved (insertion) [4]
 Formatted: Font: Not Bold
 Formatted: Font: Not Bold

258 varies between edifices (Fig. 8a), whereas determining characteristic basins by radial distance from the edifice's
 259 peak introduces geometric constraints as edifice shapes often deviate from the textbook symmetric, single-peaked
 260 edifice, instead developing large, irregular summit regions that are defined by high topography and multiple peaks
 261 (e.g., Karátson et al., 1999; Grosse et al., 2012). As slope (and thus elevation) is an essential component of erosion
 262 and basin development (Hack, 1957; Flint, 1974), we define characteristic basins as those that reach the edifice's
 263 summit region. However, we note that defining characteristic basins based on radial distance can produce different
 264 trends (Fig. S4) and may be more appropriate for some of our analyzed metrics (Section 5.3).

Deleted: vary

Deleted: (e.g., Karátson et al., 1999; Grosse et al., 2012)

Deleted:),

265 Generating a series of elevation contours along the edifice at intervals of 2.5% of the edifice's relief, we calculate
 266 the number of basins that intersect each contour, normalized by the contour's length (Fig. 2c, red line). For all
 267 edifices, we define the edifice's summit as the upper 30% of the edifice's relief, and thus consider the basins that
 268 reach this summit region (referred here as *summit basins*) as those that best characterize the edifice's drainage
 269 development. We then determine summit basin numbers, mean basin slopes (Fig. 2d), basin lengths (L_B ; Fig. 2d, red
 270 line), basin reliefs (Fig. 2e, black line), and maximum cross-basin widths (W_B ; Fig. 2e, blue line). To compare
 271 values across edifices of varying sizes, summit basin numbers are normalized by the length of the summit contour
 272 (Fig. 2c) and basin reliefs are normalized by the relief of the entire edifice. We also utilize the radial nature of
 273 edifices to generate normalized values of basin length (L'_B) and width (W'_B) as

$$274 \quad L'_B = \frac{L_B}{L_E}, \quad (3)$$

275 and

$$276 \quad W'_B = 2 \tan^{-1} \left(\frac{W_B/2}{L_{W_B}} \right), \quad (4)$$

277 respectively, where L_E is the edifice's effective radius, defined as the radius of the circle with the same planform
 278 area (A_E) as the edifice's boundary ($L_E = \sqrt{A_E / \pi}$), and L_{W_B} is the distance from the highest point within a basin to
 279 where the basin is widest. W'_B thus converts basin widths into an angle relative to the summit (Fig. 2d, light blue
 280 lines). Mean values of these quantities are then calculated for each edifice.

281 We also calculate mean summit basin hypsometry integrals for each edifice (Strahler, 1952; Fig. 2c, black lines).
 282 Individual basin hypsometry curves (H_C) are derived by counting the number of basin pixels N_{P_B} at or above
 283 normalized elevation values (Z , ranging from 0 to 1); afterwards, these values are normalized by the total number of
 284 basin pixels ($N_{P_{Tot}}$) as

$$285 \quad H_C(Z_I) = \frac{N_{P_B}(Z \geq Z_I)}{N_{P_{Tot}}}, \quad (5)$$

286 where I is a counter over normalized elevation values from 0 to 1. Hypsometry integrals of each basin are calculated
 287 as the positive integration over the curves from eq. (5). These are also averaged for each edifice.

2.3 Edifice Landform Morphology

As well as studying the temporal evolution of drainages on edifices, we also consider the broad geometry of the volcanoes. Grosse et al. (2009, 2012) developed the initial MorVolc algorithm in IDL, which quantifies edifice morphologies through a series of size, shape, slope, orientation, peak, and summit parameters. Using the same framework as DrainageVolc, we redeveloped the IDL code in Matlab, also utilizing the TopoToolbox DEM analysis package (Schwanghart and Scherler, 2014). Both DrainageVolc and the updated MorVolc scripts are available for use on GitHub (https://github.com/danjohara/Volc_Packages).

We analyze simple edifice geometry measurements with this updated version of MorVolc, including effective radius, height, height-radius ratio, and mean slope of the main flank (edifice region between the lowest closed-contour that encompasses the edifice and the summit contour, Fig. 2a). We also quantify the mean contour ellipticity and irregularity indices of the main flank from the previously-computed contours. The ellipticity index (EI) describes the elliptical nature of the edifice elevation contours, and is defined as

$$EI = \frac{\pi(L_M/2)^2}{A_C}, \quad (6)$$

where L_M is the length of the major axis of a best-fitting ellipse through the contour and A_C is the area enclosed by the contour (Grosse et al., 2012). The irregularity index (II) describes divergence of the contour from a smooth ellipse as

$$II = di_{contour}(di_{ellipse} - 1), \quad (7)$$

where di is the dissection index, defined as

$$di = \frac{P_C}{2A_C} \sqrt{A_C/\pi}, \quad (8)$$

with P_C and A_C being the perimeter and area of the contour, respectively (Grosse et al., 2012). Finally, we also incorporate new measurements within MorVolc, including the slope variance of the entire edifice (standard deviation of all slope values divided by the mean slope, similar to roughness), as well as a minimum eroded volume estimate. Eroded volume is estimated from a convex-hull reconstruction of the edifice, using the methodology described in O'Hara and Karlstrom (2023), in which the footprints of individual elevation contours along the edifice are altered to remove concave regions (assuming they represent incised topography), thus creating convex polygons. Polygons are then interpolated in three dimensions to create a simplified, reconstructed edifice. Afterwards, the current topography is subtracted from the reconstructed edifice and positive values (i.e., areas having been eroded) are integrated to estimate the volume of eroded material. Finally, eroded volume is normalized as a percent relative to the total reconstructed volume.

2.4 Edifice Ages

To explore morphological evolution through time, we correlate edifice landform and drainage basin metrics to volcano ages of activity. We thus compile known eruption records of each volcano, with ages ranging from present to early Pleistocene (Table T2). Volcanoes often have complex surface evolutions, with lifespans of activity that

Formatted: Line spacing: 1.5 lines

Deleted: edifice's

Deleted: . Afterwards

326 range 100-1000 kyrs and characterized by episodes of stochastic growth interspersed with periods of erosion during
327 quiescence (e.g., Karátson et al., 1999; Lahitte et al., 2012). Furthermore, episodes of activity are often constrained
328 to localized regions of the edifice and thus do not fully resurface the entire landform (e.g., Civico et al., 2022).

329 Similarly, erosion across the edifice is typically non-uniform as local conditions are dependent on the age and type
330 of activity, as well as microclimates (e.g., Ferrier et al., 2013; Pierson and Major, 2014; Thouret et al., 2014; Ricci et
331 al., 2015).

332 Despite the spatial and temporal heterogeneities of activity and erosion, we argue that a generalized morphologic
333 age of an edifice may be derived that quantifies the erosional state of the landform and relates to the edifice's
334 lithologic age. To account for the time differences between short-term events and the cumulative long-term history
335 on morphology, we define an edifice's age as a single value using the log-mean between the most recent eruption
336 and oldest date of activity. This definition thus accounts for the span of temporal magnitudes; however, we note that
337 using linear-mean ages produce similar results (Fig. S5) and recognize that other definitions of an edifice's
338 morphologic age are plausible (e.g., the time since the last eruption; Fig. S6). Afterwards, we analyze the temporal
339 evolution of edifice morphologies by fitting logarithmic relationships between edifice age and morphometric
340 parameters. Some volcanoes (Sumbing, Bamus, and Ulawun) have poorly-documented histories (only the most
341 recent eruption has been dated) and are therefore excluded from the regression. Conversely, Likuruanga is known to
342 have erupted only during the Pleistocene and is incorporated in the analysis.

343 3.0 Results

344 We find trends between stratovolcano age and our morphometry metrics through time (Figs. 3-4; Supplemental
345 Table T3). Considering all metrics, we find that edifice height, mean ellipticity index, normalized eroded volume,
346 Hack's Law exponent, drainage density, mean summit basin hypsometry integral, normalized basin length, and
347 normalized basin width have R^2 values ranging 0.39 – 0.77 and correlation p-values ≤ 0.05 . This list expands to
348 include effective edifice radius and mean irregularity index by removing a notable outlier (Muria, Indonesia; Fig. 4b,
349 4e), suggesting all of these metrics provide quantitative measures to characterize the overall maturity of the edifice.
350 Other metrics have weaker correlation values ($0 < r < 0.25$) and are statistically insignificant (p-values > 0.1), and thus
351 may be more sensitive to the initial edifice geometry or other processes that alter edifice morphology, or that age is
352 not a significant factor for these metrics. Muria (the noted outlier for effective edifice radius and irregularity index)
353 has an extensive volcanic history (from ~ 800 ka to 2 ka; McBirney et al., 2003; Global Volcanism Program, 2013)
354 and a morphology characterized by two broad fluvial networks on opposite flanks that are deeply incised into the
355 landform and may be associated with breached craters or flank collapses (Fig. 1a), suggesting this edifice may not fit
356 into the simple, radial volcano expectation of our dataset. We also note that due to the geometries that Acatenango
357 and Atitlán share with their sister volcanoes (Fuego and Tolimán, respectively; Fig. 1d), and our imposed definition
358 of an edifice's main flank (region between the lowest closed-contour and upper 30% of the edifice's height),
359 irregularity and ellipticity values could not be derived for these volcanoes.

360 Of the statistically-significant metrics related to edifice drainage morphology, mean summit basin hypsometry
361 integral and normalized width increase through time, whereas Hack's Law exponent, drainage density, and mean

Deleted: stochastic

Deleted: (e.g., Karátson et al., 1999; Lahitte et al., 2012)

Deleted: Similarly, erosion across the edifice is typically non-uniform as local conditions are dependent on the age and type of activity within the vicinity (e.g., Ferrier et al., 2013; Pierson and Major, 2014; Thouret et al., 2014; Ricci et al., 2015)

Deleted: S5

Formatted: Font color: Black

Deleted: only

Formatted: Font color: Black

Formatted: Font color: Black

Deleted: volcano

Deleted: morphometric

Deleted: effective edifice radius, mean irregularity index (with the exception of an outlier; Fig. 4e),

Deleted: edifice slope variance,

Deleted: 38

Deleted: 75

Deleted: < 0.1, suggesting

Deleted: .21

Deleted: 32

Deleted: with

Deleted: of

Deleted: 11 – 0.21

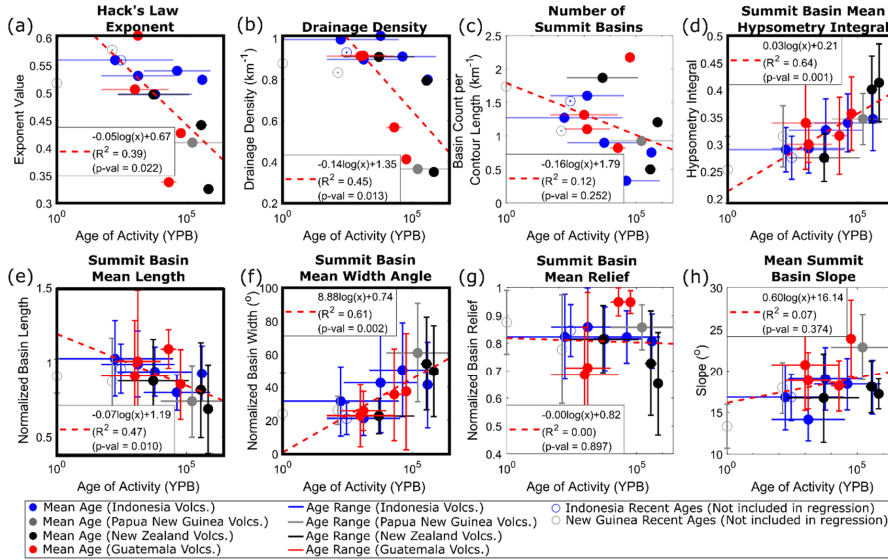
Deleted: The

Deleted: in

Deleted: is Muria (Indonesia) and originates from

Deleted:).

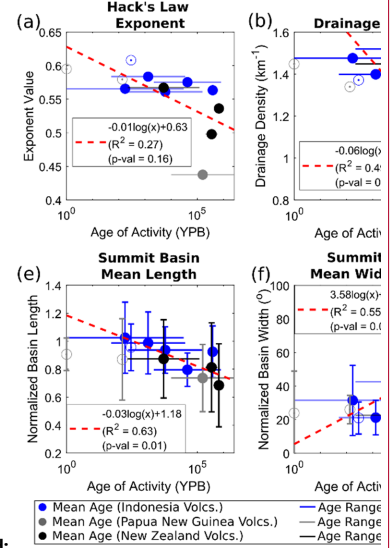
388 summit basin normalized length decrease (Fig. 3). Similarly, considering statistically-significant metrics related to
 389 the edifice as a primary landmark, mean irregularity index, mean ellipticity index, and convex-hull based eroded
 390 volumes increase with age, while edifice height and effective radius decrease with age (Fig. 4).



391
 392 **Figure 3** – Temporal relationships of drainage basin morphology metrics. Colors correspond to volcanic region. Horizontal lines
 393 are edifice age ranges of activity, with filled circles representing log-mean age. Vertical lines represent one standard deviations of
 394 values (where appropriate). Red-dashed lines and equations characterize logarithmic regressions; open circles are excluded from
 395 the regression due to age constraints. **Thick black border highlights relationships with $R^2 > 0.35$.**

Deleted: ,

Deleted: , and slope variance



Deleted:

Formatted: Font: Not Bold

Deleted: in

Formatted: Font: Not Bold

Deleted: limitations

Formatted: Font: Not Bold

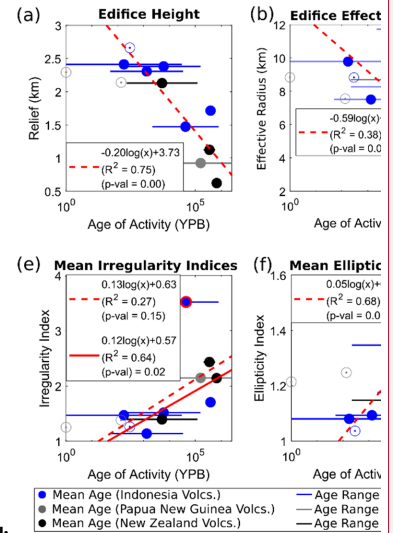
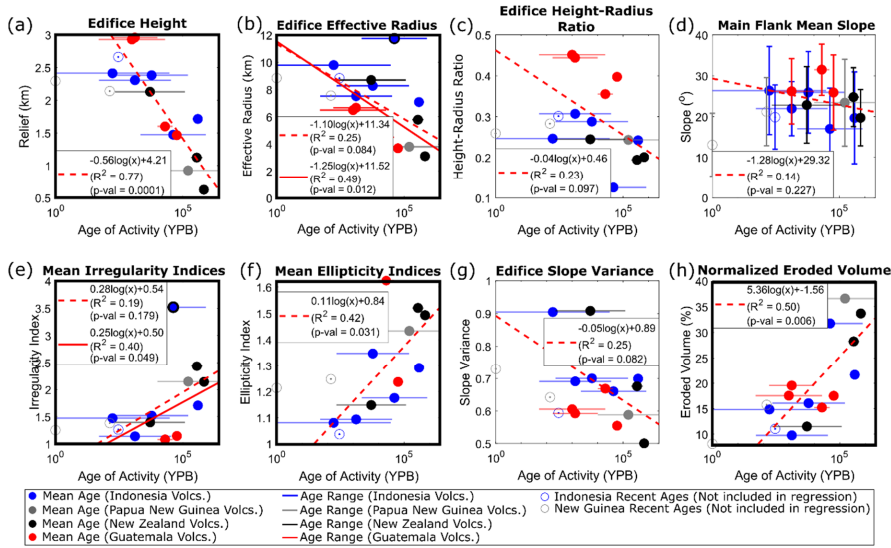


Figure 4 – Temporal relationships of landform morphology metrics. Colors and symbols are same as those described in Fig. 3. Solid red lines in (b) and (e) are secondary regressions with outlier (Muria) excluded. Thick black border highlights relationships with $R^2 > 0.35$.

4.0 Discussion

4.1 Generalized model for edifice degradation

The evolution of stratovolcanoes as primary landforms and the drainage basins that erode them are inextricably linked. Our results thus establish a new framework for evaluating volcanic edifices by considering both the landform and its drainage systems. This evolutionary model expands on stages previously defined qualitatively (Ollier, 1988) and follows similar drainage evolution observed in badlands (Schumm, 1956).

Erosion of a stratovolcano can be described within the context of our metrics by considering a simplified, conical edifice (Fig. 5). In the initial stages of erosion (Fig. 5a, equivalent to ~10% normalized eroded volume in Fig. 4h), narrow (~20° normalized width angle) and uniform (normalized mean length near 1) drainages form that extend from the summit region to the lower flanks (i.e., ‘parasol ribbing’; Ollier, 1988), giving a high drainage density (~1 km⁻¹) and Hack’s Law exponent (~0.6).

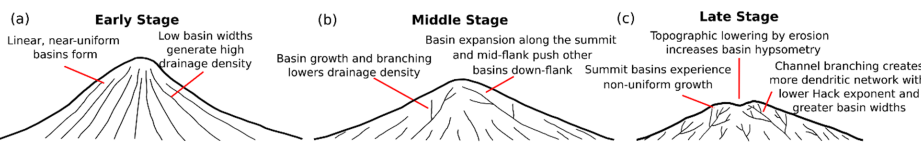


Figure 5 – Conceptual model of edifice dissection based on analysis results. Thin black lines represent drainage systems.

Deleted:

Formatted: Font: Not Bold

Deleted: line

Formatted: [7]

Deleted: is

Formatted: Font: Not Bold

Deleted: regression

Formatted: [8]

Deleted: (red circle)

Formatted: [9]

Deleted: volcanic edifices...tratovolcanoes as primary landforms and the drainage basins that erode them are inextricably linked. Our results thus establish a new framework for evaluating volcanic edifices by considering both the landform and its drainage systems. This evolutionary model expands on stages previously def...

Formatted: [10]

Deleted: volcanic edifice...tratovolcano can be described within the context of our metrics by considering a simplified, conical edifice (Fig. 5). In the initial stages of erosion...

Formatted: [11]

Deleted:

Formatted: Font: Not Bold

464

465 As the edifice degrades to 30-40% normalized eroded volume (Fig. 4h) on 10-100 kyr timescales (Fig. 5b-c), both
466 its height and area decrease; however, height decreases faster, leading to a decrease in height-radius ratios. The
467 erosion of the edifice is accompanied by drainage basin growth, with summit basins expanding azimuthally along
468 the edifice to normalized basin widths of 40-60°, pushing the headwaters of other basins down the edifice flanks.
469 Furthermore, as summit basins expand, they incise into the edifice flanks and develop a more dendritic structure
470 associated with lower drainage density ($\sim 0.5 \text{ km}^{-1}$) and Hack's Law exponent (~ 0.4). This is accompanied by non-
471 uniform summit basin growth that causes normalized basin lengths to decrease below 1.

472 As the edifice erodes, processes occur over varying scales to alter general edifice morphology: 1) over the entire
473 edifice, erosion-driven topographic lowering occurs faster than horizontal areal loss of the edifice, creating a flatter
474 landform; and 2) at the scale of a basin, incision carves into the initially-planar flanks of the edifice, steepening
475 surrounding valley walls and increasing contour irregularity. The relationship between basin-scale incision and
476 edifice-scale flattening is recorded through summit basin hypsometry integrals, with increasing values suggesting
477 that edifice-scale flattening is the dominant process. This leads to a scale-dependent behavior in edifice morphology
478 – although the edifice as a landform is becoming flatter, incision causes topography to steepen locally. Previous
479 studies (e.g., Karátson et al., 2012; Dibacto et al., 2020; Ollier, 1988) suggest this simultaneous behavior causes the
480 edifice to lose its conical, single-peaked nature over longer (> 1 Myr) timescales, developing high-relief drainage
481 divides over an extended summit region that support binary basin competition as the edifice erodes to the same relief
482 as surrounding terrain. Furthermore, we note that the decrease in edifice area through time differs from the
483 expectation of a sedimentary apron around the edifice increasing in area as the edifice erodes. Since edifice
484 boundaries are consistently defined in-part by a 3° topographic slope threshold, this suggests that on the 100 kyr
485 scale, sediment is not depositing at the edifice's base, but is being evacuated from the vicinity of the edifice, likely
486 through fluvial transport. The loss of the sedimentary apron and overall decrease in planform area as the edifice
487 transitioned from its 'intact' phase to 'planèzes' stage was also suggested by Ollier (1988).

488 This conceptual model represents a generalized view of edifice degradation, as a variety of processes (both volcanic
489 and erosional) can impact an edifice's morphology throughout its lifespan. Furthermore, other climate conditions not
490 considered here (e.g., glaciers, arid environments) are expected to alter the patterns and rates of basin evolution.
491 Nonetheless, we propose that, barring major events that significantly alter topography, stratovolcano degradation by
492 fluvial processes generally follows the model presented here.

493 4.2 How do basins compete on radial structures?

494 Our results suggest that drainages on radial structures are highly dynamic. From initially-uniform basin geometries,
495 preferential erosion causes basins near the summit to become more dominant and expand, forcing other basins
496 down-flank and generating a 'topographic hierarchy', with higher-order basins spanning the entire flank of the
497 edifice and lower-order basins occurring on lower sections, analogous to inferred basin evolution on linear fault
498 blocks (Talling et al., 1997). This hierarchy of basin ordering is a direct product of non-uniform basin development

Deleted: 1

Deleted:).

Deleted: lengthening; combined with possible volcanic activity that can influence landform asymmetry (i.e., causing a higher ellipticity index), non-uniform basin

Deleted: As the edifice erodes, processes occur over varying scales to alter general edifice morphology: 1) over the entire edifice, erosion-driven topographic lowering occurs faster than horizontal areal loss of the edifice, creating a flatter landform; and 2) at the scale of a basin, incision carves into the initially-planar flanks of the edifice, steepening surrounding valley walls and increasing contour irregularity. The relationship between basin-scale incision and edifice-scale flattening is recorded through summit basin hypsometry integrals and the slope variance of the entire edifice. The decrease in edifice slope variance suggests mean edifice slopes increase relative to the standard deviation of slope, thus suggesting overall steepening of topography. However, increasing values of summit basin hypsometry integrals suggest that edifice-scale flattening is the dominate process. This leads to a scale-dependent behavior in edifice morphology – although the edifice as a landform is becoming flatter, incision causes local relief within the bounds of the landform to become steeper.¶

Deleted: composite volcano

524 over the edifice that contributes to the preservation of less-eroded portions of the lower flanks (i.e., planèzes; Ollier,
525 1988).

526 Non-uniform basin development and transience is a natural component of landscape evolution (e.g., Hasbargen and
527 Paola, 2000); however, various factors (both volcanic and non-volcanic) can influence erosional patterns and
528 accentuate basin growth across volcanic edifices. These may include 1) local slope changes associated with
529 magmatic intrusions (e.g., Wicks et al., 2002; Biggs et al., 2010; Castro et al., 2016) or mass-wasting (e.g., Ui and
530 Glicken, 1986; Shea and van Wyk de Vries, 2008); 2) variable volcanic eruption activity that increase sediment
531 loads (Hayes et al., 2002; Pierson and Major, 2014), alter infiltration and rock erodibility (e.g., Wells et al., 1985;
532 Sklar and Dietrich, 2001; Jefferson et al., 2010), or remove bedrock through scouring by pyroclasts (Gase et al.,
533 2017) or melting by lava flows (i.e., thermal erosion; Kerr, 2001) during deposition; 3) non-uniform changes in
534 overland flow and stream power associated with breached craters (e.g., Karátson et al., 1999) or edifice-scale
535 precipitation gradients (e.g., Ferrier et al., 2013); and 4) downstream alterations to drainage channels that migrate
536 upstream as a propagating incision wave (i.e., knickpoints; Kirby et al., 2003; Cook et al., 2013; Perron and Royden,
537 2013). The long-term compilation of such processes helps drive non-uniform erosion across the edifice, which in
538 turn encourages divide migrations and changes in basin size and geometry. More specifically, basins that exhibit
539 higher erosion rates would tend to expand at the expense of their neighboring basins and potentially become the
540 dominant basins, while lower erosion rates will cause other basins to shrink and their boundaries to migrate further
541 down the edifice's flank.

542 The morphology of drainage divides is sensitive to differences in erosion between neighboring basins and can thus
543 be used to characterize basin competition. We quantify basin geometry unsteadiness through an exploration of
544 divide stability using the *divide asymmetry index (DAI)* (Forte and Whipple, 2018; Scherler and Schwanghart, 2020),
545 calculated as the positive difference in hillslope relief (vertical distance between the ridge and nearest channel)
546 across a divide and normalized by the sum of hillslope reliefs, ranging between 0 (symmetric) and 1 (asymmetric).
547 We limit our analysis to only consider divides that correspond to fluvial basins (i.e., have drainage areas $> 1.0 \text{ km}^2$
548 (Scherler and Schwanghart, 2020).

549 Divide mobility is expressed using probability density functions (PDFs) of *DAI* for all volcanoes (Fig. 6a). A clear
550 temporal trend emerges – older volcanoes have larger distributions clustered around lower (< 0.4) *DAI* that rapidly
551 decrease with increasing *DAI*; while younger volcanoes show monotonically-decreasing distributions, with fewer
552 normalized populations of low-*DAI* and greater normalized populations of high-*DAI* values compared to older
553 volcanoes. Integrating these PDFs into single values (referred to here as Γ ; Fig. 6b) shows a moderate correlation
554 with age ($R^2 = 0.38$) with the removal of Likuruanga (Papau New Guinea) as an outlier, which may be associated
555 with a breached crater (Fig. 1b).

556 Combined with basin morphology trends (Fig. 3), this suggests younger volcanoes have basins with more uniform
557 planform geometries and less-stable basin configurations. As the edifice erodes, basin planform geometries become
558 less uniform, but develop more stable configurations as evidenced by the greater symmetry of hillslope relief across

Deleted: (e.g., Wicks et al., 2002; Biggs et al., 2010; Castro et al., 2016)

Deleted: (Hayes et al., 2002; Pierson and Major, 2014)

Deleted: (e.g., Wells et al., 1985; Sklar and Dietrich, 2001; Jefferson et al., 2010)

Deleted: (e.g., Karátson et al., 1999)

Deleted: (e.g., Ferrier et al., 2013)

Deleted: Forte and Whipple, 2018; Scherler and Schwanghart, 2020)

Deleted: a Strahler order greater than

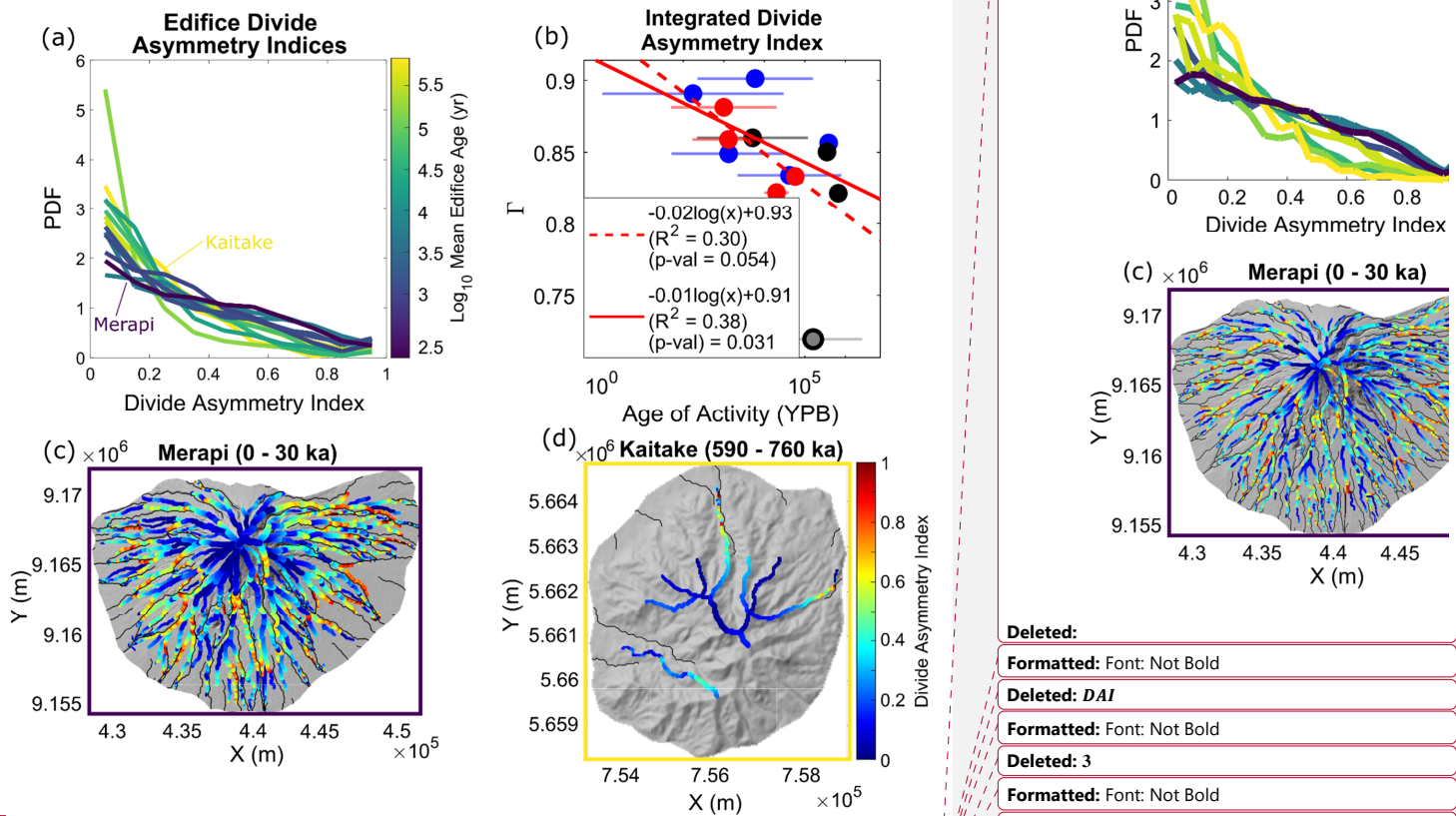
Field Code Changed

Deleted: The divide

Deleted: ($R^2 = 0.41$)

Deleted: .

572 divides. The relationship between basin non-uniformity and stability can be observed spatially by comparing *DAI*
 573 values between Merapi (youngest) and Kaitake (oldest) volcanoes (Fig. 6c-d). Highest *DAI* values on both
 574 volcanoes generally occur at the mid- and lower-flanks of the volcano, suggesting basin expansion occurs mainly
 575 azimuthally along edifice flanks, rather than across the edifice summit. This spatial analysis highlights the process
 576 that generates topographic hierarchy – by expanding azimuthally, basin growth drives less-dominant basins down-
 577 flank through a zippering process, creating drainages with tapered geometries along the lower flanks.

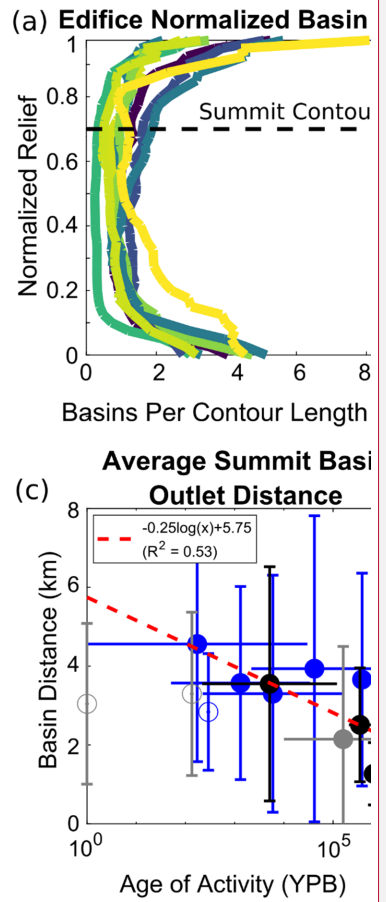
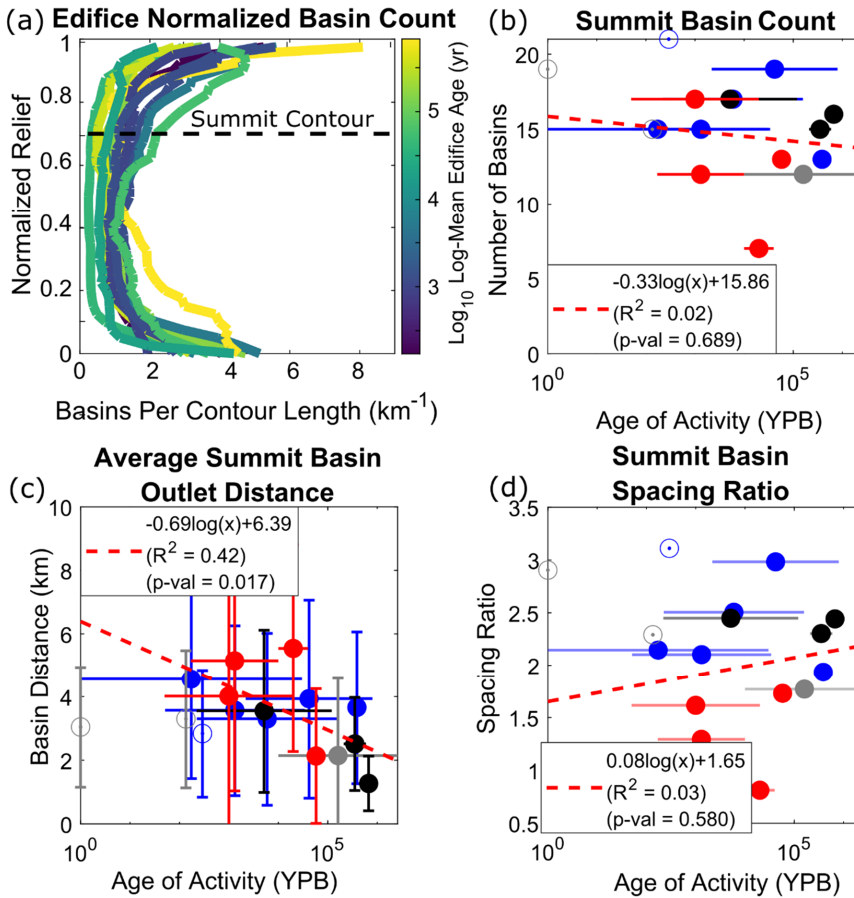


578
 579 **Figure 6 – a:** Probability density functions (PDFs) of volcano divide asymmetry indices (*DAI*); colors correspond to log-mean
 580 edifice ages. **b:** Integral of PDFs (Γ) compared to edifice age. Colors and symbols are the same as Fig. 4. **c-d:** *DAI* values for (c)
 581 Merapi and (d) Kaitake at the divides, black lines are edifice channel network. **Borders are colored with respect to Fig. 6a color**
 582 **scale.**

583 4.3 Edifice basin widths and spacing

584 Our results show that edifices experience the same morphologic trends when considering the number of basins along
 585 edifice relief (Fig. 7a): lower flanks are characterized by normalized basin numbers between 2–5 km^{-1} , main flanks
 586 are characterized by relatively consistent normalized basin numbers $< 2 \text{ km}^{-1}$, while the normalized basin numbers

594 increase near the summit (upper 30% of the edifice). This trend appears to occur largely independent of age, even
 595 within the upper flank (as demonstrated by a low R^2 value of 0.12 at the summit contour, Fig. 3c), suggesting that
 596 this morphologic trend is a direct consequence of the conical nature of volcanoes. Furthermore, non-normalized
 597 summit basin numbers also demonstrate a weak temporal trend, both at the upper 30% height designation (Fig. 7b)
 598 as well as other percentages (Fig. S7). This suggests that basins that initially form on the summit region may retain
 599 their topographic position as the edifice erodes. However, Fig. 3f demonstrates that these basins still widen through
 600 time, to a width angle of $\sim 60^\circ$, though further analysis on older volcanoes is needed to explore whether this persists
 601 on the Myr-timescale.



602 **Figure 7** **a**: Normalized number of basins along normalized relief for each volcano; colors are log-mean edifice age. **b**: Non-
 603 normalized number of summit basins (defined by the upper 30% of the edifice's height; black-dashed line of a) compared to log-
 604

Deleted: 28

Deleted: S6

Deleted: ° (

Deleted:).

Deleted:

Formatted: Font: Not Bold

Formatted: Font: Not Bold

Formatted: Font: Not Bold

610 mean edifice age. **c**: Average along-perimeter summit basin distance compared to edifice age. **d**: Summit basin spacing ratio
611 (data from Fig. 4b divided by data from c) compared to edifice age. Colors and symbols in b-d are the same as Fig. 3.

612 An apparent contradiction occurs when comparing mean summit basin width angles to the number of summit basins.

613 If all summit basins reached a width angle of $\sim 60^\circ$, it would be expected that only ~ 6 basins would exist at the

614 summit; however, Fig. 7b shows that the number of basins that reach the summit on most edifices is greater than 10.

615 This difference is a consequence of radial drainage basins achieving their maximum widths at different heights

616 relative to the height of the edifice, such that basin widths are normalized by different distances from the summit.

617 Indeed, as discussed in Section 4.2, divide asymmetry is most frequent in the mid- and lower-flanks of the edifice

618 (Fig. 6), thus accommodating largest basin widths at different sections of the flank.

619 If the number of basins that reach the summit is time invariant, how does this translate to the circumferential spacing

620 of their outlets at the base of the edifice? Hovius (1996) compiled the ratio between mountain belt half-widths

621 (distance between the major divide and mountain front, W_M) and distances between major drainage basin outlets

622 (those that reach the major divide; s) in 11 mountain ranges globally, and determined a globally-averaged spacing

623 ratio (W_M / s) of $\sim 2-3$. We perform a similar analysis by dividing edifice effective radii by the average along-

624 perimeter spacing between summit basin outlets. Figs 4b and 7c show that while edifice effective radii decrease

625 through time, so does the average perimeter distance between summit basin outlets. These behaviors thus combine

626 to produce summit basin spacing ratios of $\sim 1-3$ (Fig. 7d), consistent with Hovius (1996) as well as modeling

627 studies of drainage patterns (Habousha et al., 2023). This suggests that while summit basins azimuthally expand

628 their widths, the edifice is also decreasing in area as the landform erodes, thus decreasing the distances between

629 summit basin outlets.

630 However, a different behavior emerges when considering basins by their radial distance relative to the edifice's peak

631 (Fig. 8), which is more sensitive to the areal expansion of basins along the edifice's flank. Plotting the non-

632 normalized number of basins as a function of radial distance (normalized by maximum radius for each edifice) and

633 time shows a clear temporal trend (Fig. 8a), with younger edifices having more basins along all sections of the

634 volcano (as schematized in Fig. 5). This trend becomes more apparent through the logarithmic regression between

635 edifice age and the number of basins that exist at 30% radial distance from the peak (Fig. 8b), with other normalized

636 distances showing the same behavior (Fig. S8). Conducting a similar outlet perimeter-distance analysis on these

637 basins shows that the average distance between basin outlets is relatively constant at ~ 2 km (Fig. 8c), giving a

638 temporal decrease in basin spacing ratios ($R^2 = 0.35$, Fig. 8d). This relationship suggests a dynamic in radial

639 drainage evolution related to landform geometry. Combined with other metrics, our results suggest that as the

640 edifice erodes and loses planform area through time, very small basins on the edifice's lower flanks likely become

641 erased while more dominant basins widen on the mid flank, thus causing basins that exist within 30% radial distance

642 of the edifice's summit to retain an approximately constant outlet distance along the shrinking perimeter.

Formatted: Font: Not Bold

Formatted: Font: Not Bold

Deleted: all

Deleted: how basin widths are calculated – by normalizing basin widths as an angle

Deleted: distance from the summit to the widest part

Deleted: , basins become

Deleted: lengths corresponding to their widest regions.

Deleted: 5

Deleted: Hovius (1996) compiled the ratio between mountain belt half-widths (distance between the major divide and mountain front, W_M) and distances between major drainage basin outlets (those that reach the major divide; s) in 11 mountain ranges globally, and determined a globally-averaged spacing ratio (W_M / s) of $\sim 2-3$. We perform a similar analysis by dividing edifice effective radii by the average along-perimeter spacing between summit basin outlets. Figs 4b and 7c shows that while edifice effective radii decrease through time, so does the average perimeter distance between summit basin outlets. These behaviors thus combine to produce a relatively constant summit basin spacing ratio $\sim 1.8 - 3.1$ (Fig. 7d), consistent with Hovius (1996) as well as modeling studies of drainage patterns (Habousha et al., 2023)

Deleted: log-mean

Deleted: and at

Deleted: S7

Deleted: strong ($R^2 = 0.82$)

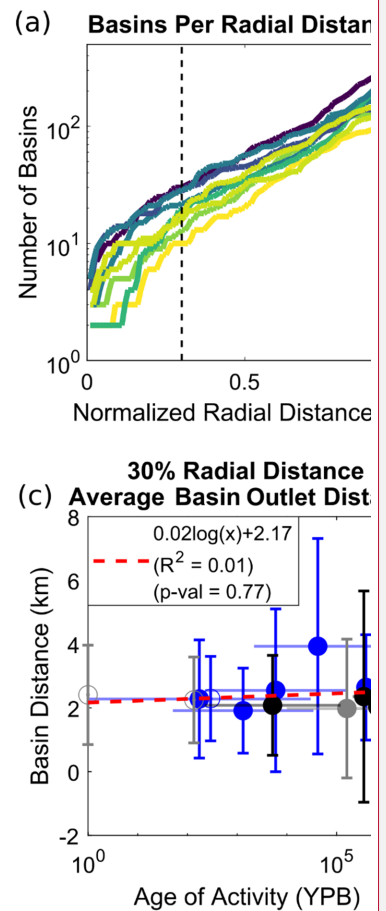
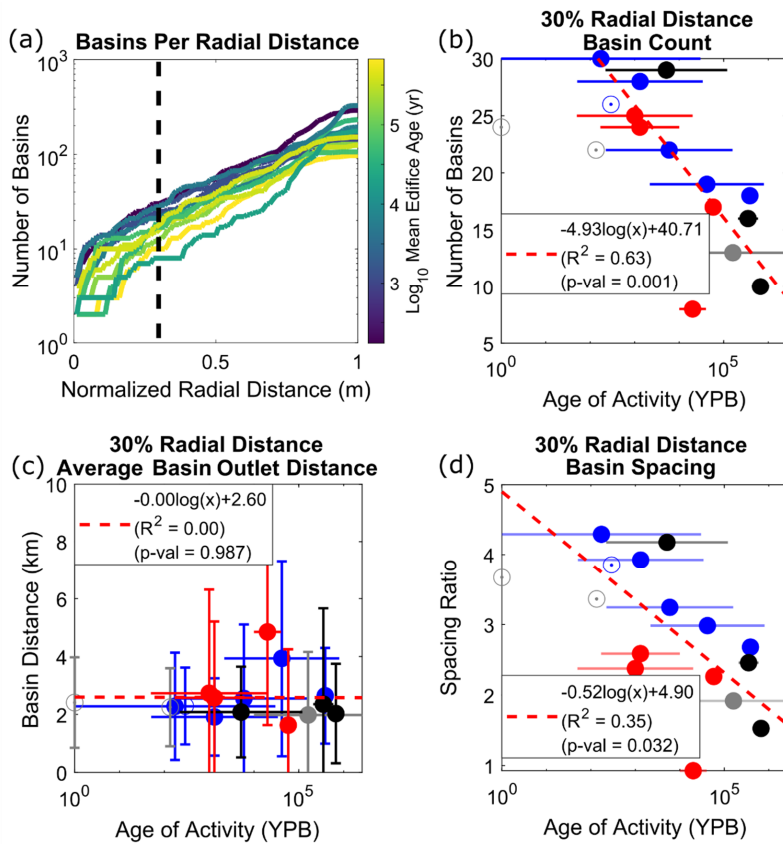
Deleted: behavior is similar to that described for the

Deleted: of basin spacing on linear fault blocks (Talling et al., 1997) and is associated

Deleted: the decreasing number of basins

Deleted: (driven by basin widening), highlighting

Deleted: evolution and dynamics of radial drainage basins on volcanic edifices



676

677 **Figure 8.** **a;** Non-normalized number of basins as a function of normalized distance from the edifice's peak; colors are log-
 678 mean edifice age, black-dashed line represents 30% normalized radial distance from the edifice's peak (basins used for plots in
 679 **b-d**). **b;** Non-normalized number of basins compared to log-mean edifice age. **c;** Average along-perimeter basin distance
 680 compared to edifice age. **d;** Basin spacing ratio (data from Fig. 4b divided by data from c) compared to edifice age. Colors and
 681 symbols in b-d are the same as Fig. 3.

682 4.4 Radial drainage basin area-length relationship

683 As a final observation for volcanic edifice drainage basins, we consider basin geometries in reference to Hack's
 684 power-law relationships between basin areas and lengths (Hack, 1957). Analyzing Hack's Law regressions for
 685 Merapi and Kaitake (Fig. 9), the relationships between spatial location and basin geometries become apparent. On
 686 Merapi, basins less than 10^5 m^2 do not conform to the same power-law trend as those greater than 10^5 m^2 , whereas
 687 on Kaitake this break occurs at 10^6 m^2 . These smaller basins are constrained to the lowest regions of the edifice's
 688 flank and likely correspond to non-channeled surfaces. Of those considered for the Hack's Law regression, the log₁₀
 689 basin length deviation (D_L) from the power-law is calculated as

Deleted:

Formatted

... [12]

Deleted: .

Formatted

... [13]

Deleted: within 30% of the edifice's peak (black-dashed line of a)

Formatted

... [14]

Deleted: Our analysis indicates that basins with drainage areas greater than 10^5 m^2 are well-fit by a power-law regression (Figs. 2b, 9a, c), whereas basins smaller than 10^5 m^2 have steeper trends between basin area and length, and are likely non-fluvial within the bounds of the edifice. Analyzing Hack's Law regressions for Merapi and Kaitake (Fig. 9), the relationships between spatial location and basin geometries become apparent. Basins that are...n Mer[... [15]

727 $D_L = \log_{10}(L_H(A)) - \log_{10}(L),$ (9)

728 where L_H is the basin length of the Hack's Law regression from a given basin's area (A), and L is the basin's length.
729 As expected from the geometric relationship, basins that fall below the power-law regression ($D_L < 0$) are wider,
730 and those that are above the power-law regression ($D_L > 0$) are narrower.

731 Calculating D_L for basins with areas greater than our imposed channelization threshold (1.0 km²), one clear
732 observation is the presence of highly-elongated basins on Merapi that exist on the mid- to upper-flanks and have D_L
733 values > 0.15 (Fig. 9c). These basins appear wedged or pinched between larger basins and would be expected to not
734 have as much growth potential compared to their wider neighbors. Elongated basins also exist on Kaitake; however,
735 they do not have as high of a deviation (maximum $D_L \approx 0.1$; Fig. 9d). This may be a product of the lower number of
736 basins that exist on Kaitake, the overall lower amount of drainage area that Kaitake basins occupy, or an evolution
737 of basins towards more consistent patterns, thus decreasing the amount of variability from the power-law
738 relationship. On both Merapi and Kaitake, these elongated basins may further highlight the dynamics of basin
739 competition on radial structures – through drainage divide migration and areal loss (likely influenced by edifice-
740 scale sector collapses or regrowth events; Gertisser et al., 2023), less-erosive drainages become passive players to
741 more dominant basins and adopt non-standard geometries, becoming narrow, chute-like basins on the mid- and
742 upper-flanks.

Deleted: 0.5 km²), we do not observe any specific spatial pattern related to basins that deviate above or below the Hack's Law regression. However,

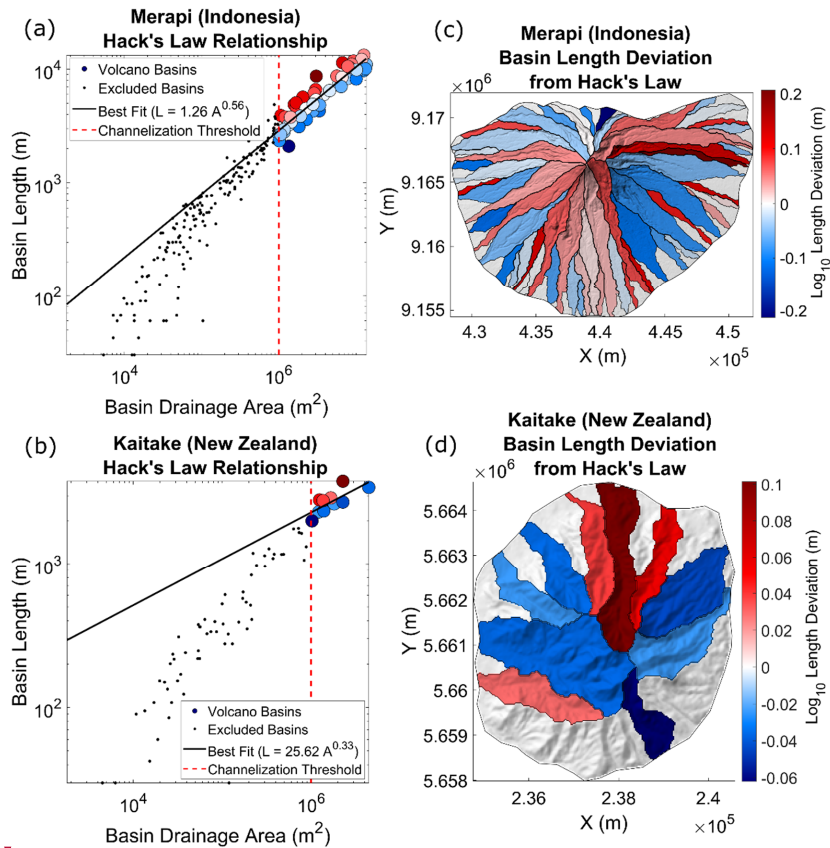
Deleted: 2

Deleted: 9b

Deleted: or

Deleted:

Deleted: and lower-order drainages become passive players to more dominant basins and adopt non-standard geometries, becoming narrow, chute-like basins on the mid- and upper-flanks. The generation of these narrow, 'nested' basins has also been observed to occur in response to differential tectonic uplift within analog and numerical experiments (Habousha et al., 2023).



757

758 **Figure 9** Hack's Law analysis of (a, c) Merapi and (b, d) Kaitake. a, b: Basin drainage area – length relationships. Black lines
 759 represent Hack's Law regressions. Colored circles correspond to the deviation from the regression trend (eq. 9), associated with
 760 the color bars in c and d. Red-dashed line is imposed 1.0 km² channelization threshold, black dots are basins less than the
 761 threshold and excluded from the regression. c, d: Maps showing the deviation of each basin from the best-fit power-law
 762 regression.

763 **4.5 How do radial drainages compare to other settings?**

764 Thus far, our discussion has focused on deriving a foundational understanding of how radial drainages on volcanic
 765 edifices evolve and compete. However, we note similarities between our interpretation and those from previous
 766 studies in other drainage settings. This leads to a simple question – is there a significant difference between radial
 767 and dendritic drainage development and evolution?

768 Our results show that basin formation on volcanic edifices follows the development of rills and gullies within
 769 badlands (Schumm, 1956). As radial drainages evolve and certain basins expand to become dominant features on the
 770 edifice, less-dominant basins become passive and are pushed down-flank, often adhering to non-standard geometries

(a) **Merapi (Indonesia)**
Hack's Law Relationship

(c) **Merapi (Indonesia)**
Basin Length Deviation from Hack's Law

(b) **Kaitake (New Zealand)**
Hack's Law Relationship

(d) **Kaitake (New Zealand)**
Basin Length Deviation from Hack's Law

Deleted:

Formatted: Font: Not Bold

Deleted: -b

Formatted: Font: Not Bold

Deleted: -c

Formatted: Font: Not Bold

Deleted: , c

Formatted: Font: Not Bold

Deleted: b

Formatted: ... [16]

Deleted: .5

Formatted: Font: Not Bold

Deleted: b,

Formatted: Font: Not Bold

Deleted: as nested basins

787 as imposed by their more-dominant neighbors (Habousha et al., 2023; Beeson and McCoy, 2022). The dynamics of
788 this basin competition and formation of passive basins are demonstrated by edifice basin spacing ratios. Summit
789 basins on edifices have spacing ratios that appear time-independent and fit within the range of values observed in
790 linear mountain ranges globally (Hovius, 1996) (Fig. 7), suggesting this ratio is set during the initial stages of basin
791 formation – an attribute of basin evolution that has been shown to occur on linear fault blocks (Talling et al., 1997;
792 Habousha et al., 2023). However, basins that are within a radial distance from the summit that is 30% of the
793 edifice’s maximum radius do experience a temporally-decreasing spacing ratio and constant distance between
794 outlets (Fig. 8), capturing the development of a basin topographic hierarchy along the edifice – a behavior not
795 previously observed. Finally, our drainage divide analysis on volcanic edifices suggest that radial drainage basins
796 evolve towards a stable basin configuration as topography matures towards a dynamic equilibrium, similar to
797 regional landscape evolution globally (e.g., Perron and Royden, 2013; Willett et al., 2014).

798 This comparison suggests that drainage development and evolution on radial structures are largely similar to those
799 occurring within linear mountain settings. However, some differences still occur, particularly in relation to basin
800 geometries imposed by the larger-scale, radial primary landform. Dendritic drainages in linear mountain belts and
801 fault blocks are characterized by their leaf-like geometries (e.g., Zernitz, 1932; Strahler, 1952; Talling et al., 1997),
802 having a broad headwater region that decreases towards the outlet to a tapered point. Although radial drainages also
803 have tapered outlets and basin widths increase upstream, these widths are hindered by the conical geometry of the
804 primary landform and convergence of multiple basins towards the summit, leading to a tapered headwater as well as
805 a tapered outlet. This geometric constraint is well-demonstrated by the drainages on Merapi (Fig. 9c), where summit
806 basins are generally widest on the lower- or mid-flanks; however, this trend is not as obvious on Kaitake (Fig. 9d),
807 where erosion has dissected the landform and weakened the conical influence of the edifice on basin geometries.

808 Furthermore, as edifice drainages are limited to a conical landform, their evolution and configuration are constrained
809 by a cumulative areal limit. As opposed to linear mountain ranges (where a morphologic change in one basin
810 impacts its neighbors, which then impacts their neighbors as a cascading chain across the landscape), on volcanic
811 edifices, a morphologic change in one basin (particularly a dominant basin) may directly impact the erosional state
812 and morphology of most other basins on the landform due to the high number of basins that may share a divide with
813 this basin. This areal effect on radial basin evolution may be further augmented by the higher diversity of underlying
814 host rocks between edifice basins associated with magmatic and volcanic products (e.g., tephra deposits, lava flows,
815 and intrusions) that is not as prevalent within linear mountain ranges.

816 Despite the differences in basin geometries and interactions discussed above, edifice-averaged morphometric values
817 (e.g., Hack’s Law exponent, drainage density, mean basin hypsometry, mean basin slopes) are similar to those of
818 other settings (Hack, 1957; Strahler, 1952; Horton, 1945). This suggests that although radial drainages experience
819 phenomena that differ from those typically experienced in dendritic settings, drainage development, geometries, and
820 competition largely follow those of dendritic patterns. As volcanic surfaces are easily datable and their ages can
821 often vary by orders magnitude on a single edifice, volcanoes thus represent ideal locations for studying terrain
822 evolution over varying temporal scales within a general framework.

Deleted: nested

Deleted: is

Deleted: (Hovius, 1996)

Deleted: the spacing of these basins

Deleted: ; however

Deleted: 9b

Deleted: an isolated,

830 **4.6 Basin morphology capturing volcanic processes**

831 In this study, we considered edifice morphologies using mean values over the entire edifice. However, our metrics
832 also allow for the comparison of basin morphologies on a single edifice. Variations associated with these metrics
833 would likely relate to spatially-localized attributes of aggradation, degradation, and climate, and would thus provide
834 a quantitative method to disentangle these signals using topography. For example, edifice flanks that have been
835 resurfaced by large volcanic deposits or destroyed by sector collapses should exhibit younger drainage networks
836 according to the metrics explored here, ~~and are expected to~~ differ from other parts of the volcano. Furthermore,
837 alterations to the erosional efficiency of a basin by tephra accumulation or lava flow emplacement should create
838 spatial variability that can be quantified by similar analyses. These concepts should be tested over well-constrained
839 cases and would be beneficial for both preliminary fieldwork and to approximate relative volcanic chronologies
840 remotely. Our model for edifice degradation, radial drainage evolution, and divide stability thus provides a first step
841 to deconvolving the various signals that relate to edifice morphology. This presents new avenues of exploration for
842 the volcanology community to interrogate volcanic histories from topography, and for the geomorphic community to
843 investigate surface evolution on landforms that often fall outside standard tectonic studies.

Deleted: that

844 **5.0 Conclusion**

845 Volcanic edifices represent a class of primary landforms whose erosion remains relatively unexplored. We analyzed
846 the degradational histories of stratovolcanoes using a set of metrics that have not previously been considered for
847 radial drainage networks. We show that these metrics relate to the overall age of a volcano and propose a new
848 general model for the temporal evolution of edifice drainage morphology. Divide stability analysis underscores the
849 dynamic nature of basin evolution, and suggests that radial drainage networks initiate with nearly-uniform
850 geometries and unstable configurations that evolve towards non-uniform basin geometries and more stable
851 configurations to generate a basin topographic hierarchy on volcanoes. Finally, comparing basin geometries,
852 configurations, and outlet spacing between basins that exist on volcanic edifices to those that exist on linear
853 mountain ranges highlights similarities and differences between radial and dendritic drainage basins.

Deleted: volcanic edifices

854 **6.0 Code availability**

855 DrainageVolc and MorVolc codes are available at https://github.com/danjohara/Volc_Packages.

856 **7.0 Data availability**

857 Collected edifice data is included in the supplement as both an Excel file and shapefile.

858 **8.0 Author contribution**

859 All authors provided editorial advice on the manuscript. DO'H wrote the DrainageVolc and updated MorVolc codes,
860 conducted the morphology analyses, and wrote the manuscript. RMJvW assisted in data collection, determined
861 edifice boundaries from topography, and tested DrainageVolc/MorVolc. LG and BC gave advice on drainage basin
862 morphology and evolution, while PG, PL, and GK provided insight on volcanic edifice morphology, evolution, and
863 general volcano ages. MK secured funds and coordinated the project, giving advice on the research direction,
864 analyses, and interpretation.

867 **9.0 Competing interests**

868 The authors declare that they have no conflict of interest.

869 **10.0 Acknowledgement**

870 This research was funded through the EVOlVe project, Junior FWO project grant G029820N of the Fonds

871 Wetenschappelijke Onderzoek – Vlaanderen.

872 **11.0 References**

- 873 Becerril, L., Lara, L. E., and Astudillo, V. I.: The strong competition between growth and erosive processes on the
874 Juan Fernández Archipelago (SE Pacific, Chile), *Geomorphology*, 373, 107513,
875 <https://doi.org/10.1016/j.geomorph.2020.107513>, 2021.
- 876 Beeson, H. W. and McCoy: Disequilibrium river networks dissecting the western slope of the Sierra Nevada,
877 California, USA, record significant late Cenozoic tilting and associated surface uplift, *Bull. Geol. Soc. Am.*, 134,
878 2809–2853, <https://doi.org/10.1130/B36517.1>, 2022.
- 879 Biggs, J., Mothes, P., Ruiz, M., Amelung, F., Dixon, T. H., Baker, S., and Hong, S. H.: Stratovolcano growth by co-
880 eruptive intrusion: The 2008 eruption of Tungurahua Ecuador, *Geophys. Res. Lett.*, 37,
881 <https://doi.org/10.1029/2010GL044942>, 2010.
- 882 Bishop, P.: Drainage rearrangement by river capture, beheading and diversion, *Prog. Phys. Geogr.*, 19, 449–473,
883 1995.
- 884 Bohnenstiehl, D. W. R., Howell, J. K., White, S. M., and Hey, R. N.: A modified basal outlining algorithm for
885 identifying topographic highs from gridded elevation data, Part 1: Motivation and methods, *Comput. Geosci.*, 49,
886 308–314, <https://doi.org/10.1016/j.cageo.2012.04.024>, 2012.
- 887 Braun, J.: A review of numerical modeling studies of passive margin escarpments leading to a new analytical
888 expression for the rate of escarpment migration velocity, *Gondwana Res.*, 53, 209–224,
889 <https://doi.org/10.1016/j.gr.2017.04.012>, 2018.
- 890 Castellort, S. and Simpson, G.: River spacing and drainage network growth in widening mountain ranges, *Basin*
891 *Res.*, 18, 267–276, <https://doi.org/10.1111/j.1365-2117.2006.00293.x>, 2006.
- 892 Castellort, S., Simpson, G., and Darrioulat, A.: Slope-control on the aspect ratio of river basins, *Terra Nov.*, 21,
893 265–270, <https://doi.org/10.1111/j.1365-3121.2009.00880.x>, 2009.
- 894 Castellort, S., Goren, L., Willett, S. D., Champagnac, J. D., Herman, F., and Braun, J.: River drainage patterns in
895 the New Zealand Alps primarily controlled by plate tectonic strain, *Nat. Geosci.*, 5, 744–748,
896 <https://doi.org/10.1038/ngeo1582>, 2012.
- 897 Castro, J. M., Cordonnier, B., Schipper, C. I., Tuffen, H., Baumann, T. S., and Feisel, Y.: Rapid laccolith intrusion
898 driven by explosive volcanic eruption, *Nat. Commun.*, 7, 1–7, <https://doi.org/10.1038/ncomms13585>, 2016.
- 899 Civico, R., Ricci, T., Scarlato, P., Taddeucci, J., Andronico, D., Del Bello, E., D’Auria, L., Hernández, P. A., and
900 Pérez, N. M.: High-resolution Digital Surface Model of the 2021 eruption deposit of Cumbre Vieja volcano, La
901 Palma, Spain, *Sci. Data*, 9, 1–7, <https://doi.org/10.1038/s41597-022-01551-8>, 2022.
- 902 Cook, K. L., Turowski, J. M., and Hovius, N.: A demonstration of the importance of bedload transport for fluvial
903 bedrock erosion and knickpoint propagation, *Earth Surf. Process. Landforms*, 38, 683–695,
904 <https://doi.org/10.1002/esp.3313>, 2013.
- 905 [Dibacto, S., Lahitte, P., Karátson, D., Hencz, M., Szakács, A., Biró, T., Kovács, I., and Veres, D.: Growth and](#)
906 [erosion rates of the East Carpathians volcanoes constrained by numerical models: Tectonic and climatic](#)
907 [implications, *Geomorphology*, 368, 107352, <https://doi.org/10.1016/j.geomorph.2020.107352>, 2020.](#)
- 908 Duvall, A. R. and Tucker, G. E.: Dynamic Ridges and Valleys in a Strike-Slip Environment, *J. Geophys. Res. F*
909 *Earth Surf.*, 120, 2016–2026, <https://doi.org/10.1002/2015JF003618>, 2015.

910 Euillades, L. D., Grosse, P., and Euillades, P. A.: NETVOLC: An algorithm for automatic delimitation of volcano
911 edifice boundaries using DEMs, *Comput. Geosci.*, 56, 151–160, <https://doi.org/10.1016/j.cageo.2013.03.011>, 2013.

912 Farr, T. G., Rosen, P. A., Caro, E., Crippen, R., Duren, R., Hensley, S., Kobrick, M., Paller, M., Rodriguez, E.,
913 Roth, L., Seal, D., Shaffer, S., Shimada, J., Umland, J., Werner, M., Oskin, M., Burbank, D., and Alsdorf, D.: The
914 Shuttle Radar Topography Mission, *Rev. Geophys.*, 45, 1–43, 2007.

915 Ferrier, K. L., Huppert, K. L., and Perron, J. T.: Climatic control of bedrock river incision, *Nature*, 496, 206–209,
916 <https://doi.org/10.1038/nature11982>, 2013.

917 Flint, J. J.: Stream gradient as a function of order, magnitude, and discharge, *Water Resour. Res.*, 10, 969–973,
918 <https://doi.org/10.1029/WR010i005p00969>, 1974.

919 Forte, A. M. and Whipple, K. X.: Criteria and tools for determining drainage divide stability, *Earth Planet. Sci. Lett.*,
920 493, 102–117, <https://doi.org/10.1016/j.epsl.2018.04.026>, 2018.

921 Fox, M., Goren, L., May, D. A., and Willett, S. D.: Inversion of fluvial channels for paleorock uplift rates in Taiwan,
922 *J. Geophys. Res. Earth Surf.*, 119, 1853–1875, <https://doi.org/10.1002/2014JF003196>, 2014.

923 Gase, A. C., Brand, B. D., and Bradford, J. H.: Evidence of erosional self-channelization of pyroclastic density
924 currents revealed by ground-penetrating radar imaging at Mount St. Helens, Washington (USA), *Geophys. Res.*
925 *Lett.*, 44, 2220–2228, <https://doi.org/10.1002/2016GL072178>, 2017.

926 Gertisser, R., Troll, V. R., Walter, T. R., Nandaka, I. G. M. A., and Ratdomopurbo, A.: Merapi Volcano: Geology,
927 Eruptive Activity, and Monitoring of a High-Risk Volcano, Springer Nature, 2023.

928 Gilbert, G. K.: The Convexity of Hilltops, *J. Geol.*, 17, 344–350, 1909.

929 [Global Volcanism Program: Volcanoes of the World, v. 4.10.5 \(27 Jan 2022\), Smithsonian Inst., 2013.](#)

930 Grosse, P., van Wyk de Vries, B., Petrinovic, I. A., Euillades, P. A., and Alvarado, G. E.: Morphometry and
931 evolution of arc volcanoes, *Geology*, 37, 651–654, <https://doi.org/10.1130/G25734A.1>, 2009.

932 Grosse, P., van Wyk de Vries, B., Euillades, P. A., Kervyn, M., and Petrinovic, I. A.: Systematic morphometric
933 characterization of volcanic edifices using digital elevation models, *Geomorphology*, 136, 114–131,
934 <https://doi.org/10.1016/j.geomorph.2011.06.001>, 2012.

935 [Haapala, J. M., Escobar Wolf, R., Vallance, J. W., Rose, W. I., Griswold, J. P., Schilling, S. P., Ewert, J. W., and](#)
936 [Mota, M.: Volcanic Hazards at Atitlán Volcano, Guatemala, Open-File Rep., 2005.](#)

937 Habousha, K., Goren, L., Nativ, R., and Gruber, C.: Plan-Form Evolution of Drainage Basins in Response to
938 Tectonic Changes: Insights From Experimental and Numerical Landscapes, *J. Geophys. Res. Earth Surf.*, 128, 1–24,
939 <https://doi.org/10.1029/2022jf006876>, 2023.

940 Hack, J. T.: Studies of longitudinal stream profiles in Virginia and Maryland, USGS Prof. Pap. 249, 97, 1957.

941 Hamawi, M., Goren, L., Mushkin, A., and Levi, T.: Rectangular drainage pattern evolution controlled by pipe cave
942 collapse along clastic dikes, the Dead Sea Basin, Israel, *Earth Surf. Process. Landforms*, 47, 936–954,
943 <https://doi.org/10.1002/esp.5295>, 2022.

944 Han, J., Gasparini, N. M., and Johnson, J. P. L.: Measuring the imprint of orographic rainfall gradients on the
945 morphology of steady-state numerical fluvial landscapes, *Earth Surf. Process. Landforms*, 40, 1334–1350,
946 <https://doi.org/10.1002/esp.3723>, 2015.

947 Hasbargen, L. E. and Paola, C.: Landscape instability in an experimental drainage basin, *Geology*, 28, 1067–1070,
948 [https://doi.org/10.1130/0091-7613\(2000\)28<1067:LIIAED>2.0.CO;2](https://doi.org/10.1130/0091-7613(2000)28<1067:LIIAED>2.0.CO;2), 2000.

949 Hayes, S. K., Montgomery, D. R., and Newhall, C. G.: Fluvial sediment transport and deposition following the 1991
950 eruption of Mount Pinatubo, *Geomorphology*, 45, 211–224, [https://doi.org/10.1016/S0169-555X\(01\)00155-6](https://doi.org/10.1016/S0169-555X(01)00155-6), 2002.

951 Horton, R. E.: Erosional development of streams and their drainage basins; hydrological approach to quantitative
952 morphology, *Geol. Soc. Am. Bull.*, 56, 275–370, <https://doi.org/10.1130/0016->

953 7606(1945)56[275:EDOSAT]2.0.CO;2, 1945.

954 Hovius, N.: Regular spacing of drainage outlets from linear mountain belts, *Basin Res.*, 8, 29–44,
955 <https://doi.org/10.1111/j.1365-2117.1996.tb00113.x>, 1996.

956 Howard, A. D.: Drainage Analysis in Geologic Interpretation: A Summation, *Am. Assoc. Pet. Geol. Bull.*, 51,
957 <https://doi.org/10.1306/5d25c26d-16c1-11d7-8645000102c1865d>, 1967.

958 Jefferson, A., Grant, G. E., Lewis, S. L., and Lancaster, S. T.: Coevolution of hydrology and topography on a basalt
959 landscape in the Oregon Cascade Range, USA, *Earth Surf. Process. Landforms*, 35, 803–816,
960 <https://doi.org/10.1002/esp.1976>, 2010.

961 Karátson, D., Thouret, J. C., Moriya, I., and Lomoschitz, A.: Erosion calderas: Origins, processes, structural and
962 climatic control, *Bull. Volcanol.*, 61, 174–193, <https://doi.org/10.1007/s004450050270>, 1999.

963 Karátson, D., Telbisz, T., and Wörner, G.: Erosion rates and erosion patterns of Neogene to Quaternary
964 stratovolcanoes in the Western Cordillera of the Central Andes: An SRTM DEM based analysis, *Geomorphology*,
965 139–140, 122–135, <https://doi.org/10.1016/j.geomorph.2011.10.010>, 2012.

966 Kerr, R. C.: Thermal erosion by laminar lava flows, *J. Geophys. Res. B Solid Earth*, 106, 453–465,
967 <https://doi.org/10.1029/2001JB000227>, 2001.

968 Kirby, E. and Whipple, K. X.: Expression of active tectonics in erosional landscapes, *J. Struct. Geol.*, 44, 54–75,
969 <https://doi.org/10.1016/j.jsg.2012.07.009>, 2012.

970 Kirby, E., Whipple, K. X., Tang, W., and Chen, Z.: Distribution of active rock uplift along the eastern margin of the
971 Tibetan Plateau: Inferences from bedrock channel longitudinal profiles, *J. Geophys. Res. Solid Earth*, 108,
972 <https://doi.org/10.1029/2001JB000861>, 2003.

973 Lahitte, P., Samper, A., and Quidelleur, X.: DEM-based reconstruction of southern Basse-Terre volcanoes
974 (Guadeloupe archipelago, FWI): Contribution to the Lesser Antilles Arc construction rates and magma production,
975 *Geomorphology*, 136, 148–164, <https://doi.org/10.1016/j.geomorph.2011.04.008>, 2012.

976 [Locke, C. A. and Cassidy, J.: Egmont Volcano, New Zealand: Three-dimensional structure and its implications for](#)
977 [evolution, *J. Volcanol. Geotherm. Res.*, 76, 149–161, \[https://doi.org/10.1016/S0377-0273\\(96\\)00074-1\]\(https://doi.org/10.1016/S0377-0273\(96\)00074-1\), 1997.](#)

978 Lohse, K. A. and Dietrich, W. E.: Contrasting effects of soil development on hydrological properties and flow paths,
979 [*Water Resour. Res.*, 41, 1–17, <https://doi.org/10.1029/2004WR003403>, 2005.](#)

980 [Major, J. J., Mosbrucker, A. R., and Spicer, K. R.: Sediment erosion and delivery from Toutle River basin after the](#)
981 [1980 eruption of Mount St. Helens: A 30-year perspective, *Ecol. Responses Mt. St. Helens Revisit. 35 years after*](#)
982 [1980 Erupt., 19–44, \[https://doi.org/10.1007/978-1-4939-7451-1_2\]\(https://doi.org/10.1007/978-1-4939-7451-1_2\), 2018.](#)

983 [McBirney, A. R., Serva, L., Guerra, M., and Connor, C. B.: Volcanic and seismic hazards at a proposed nuclear](#)
984 [power site in central Java, *J. Volcanol. Geotherm. Res.*, 126, 11–30, \[https://doi.org/10.1016/S0377-0273\\(03\\)00114-\]\(https://doi.org/10.1016/S0377-0273\(03\)00114-8\)](#)
985 [8, 2003.](#)

986 Mejía, A. I. and Niemann, J. D.: Identification and characterization of dendritic, parallel, pinnate, rectangular, and
987 trellis networks based on deviations from planform self-similarity, *J. Geophys. Res. Earth Surf.*, 113, 1–21,
988 <https://doi.org/10.1029/2007JF000781>, 2008.

989 Montgomery, D. R. and Dietrich, W. E.: Landscape Dissection and Drainage Area-Slope Threshold, in: *Process*
990 *Models and Theoretical Geomorphology*1, 1994.

991 Mudd, S. M. and Furbish, D. J.: Responses of soil-mantled hillslopes to transient channel incision rates, *J. Geophys.*
992 *Res. Earth Surf.*, 112, 1–12, <https://doi.org/10.1029/2006JF000516>, 2007.

993 Mueller, J. E.: Re-evaluation of the relationship of master streams and drainage basins, *Bull. Geol. Soc. Am.*, 83,
994 3471–3474, [https://doi.org/10.1130/0016-7606\(1972\)83\[3471:ROTROM\]2.0.CO;2](https://doi.org/10.1130/0016-7606(1972)83[3471:ROTROM]2.0.CO;2), 1972.

995 [Mulyaningsih, S. and Shaban, G.: Geochemistry of basaltic Merbabu volcanic rocks, Central Java, Indonesia,](#)

Deleted: 41

997 [Indones. J. Geosci., 7, 161–178, https://doi.org/10.17014/ijog.7.2.161-178, 2020.](https://doi.org/10.17014/ijog.7.2.161-178)

998 O'Hara, D. and Karlstrom, L.: The arc-scale spatial distribution of volcano erosion implies coupled magmatism and
999 regional climate in the Cascades arc, United States, *Front. Earth Sci.*, 11, 1–15,
1000 <https://doi.org/10.3389/feart.2023.1150760>, 2023.

1001 O'Hara, D., Karlstrom, L., and Roering, J. J.: Distributed landscape response to localized uplift and the fragility of
1002 steady states, *Earth Planet. Sci. Lett.*, 506, 243–254, <https://doi.org/10.1016/j.epsl.2018.11.006>, 2019.

1003 O'Hara, D., Karlstrom, L., and Ramsey, D. W.: Time-evolving surface and subsurface signatures of Quaternary
1004 volcanism in the Cascades arc, *Geology*, 49, e526, <https://doi.org/10.1130/g47706.1>, 2020.

1005 Ollier, C.: *Volcanoes*, edited by: Blackwell, B., Oxford., 288 pp., 1988.

1006 Perron, J. T. and Royden, L.: An integral approach to bedrock river profile analysis, *Earth Surf. Process. Landforms*,
1007 38, 570–576, <https://doi.org/10.1002/esp.3302>, 2013.

1008 Pierson, T. C. and Major, J. J.: Hydrogeomorphic effects of explosive volcanic eruptions on drainage basins, *Annu.*
1009 *Rev. Earth Planet. Sci.*, 42, 469–507, <https://doi.org/10.1146/annurev-earth-060313-054913>, 2014.

1010 Prince, P. S. and Spotila, J. A.: Evidence of transient topographic disequilibrium in a landward passive margin river
1011 system: Knickpoints and paleo-landscapes of the New River basin, southern Appalachians, *Earth Surf. Process.*
1012 *Landforms*, 38, 1685–1699, <https://doi.org/10.1002/esp.3406>, 2013.

1013 Ricci, J., Lahitte, P., and Quidelleur, X.: Construction and destruction rates of volcanoes within tropical
1014 environment: Examples from the Basse-Terre Island (Guadeloupe, Lesser Antilles), *Geomorphology*, 228, 597–607,
1015 <https://doi.org/10.1016/j.geomorph.2014.10.002>, 2015.

1016 Scherler, D. and Schwanghart, W.: Drainage divide networks - Part 1: Identification and ordering in digital elevation
1017 models, *Earth Surf. Dyn.*, 8, 245–259, <https://doi.org/10.5194/esurf-8-245-2020>, 2020.

1018 Schumm, S. A.: Evolution of drainage systems and slopes in badlands at Perth Amboy, New Jersey, *Bull. Geol. Soc.*
1019 *Am.*, 67, 597–646, [https://doi.org/10.1130/0016-7606\(1956\)67\[597:EODSAS\]2.0.CO;2](https://doi.org/10.1130/0016-7606(1956)67[597:EODSAS]2.0.CO;2), 1956.

1020 Schwanghart, W. and Scherler, D.: Short Communication: TopoToolbox 2 - MATLAB-based software for
1021 topographic analysis and modeling in Earth surface sciences, *Earth Surf. Dyn.*, 2, 1–7, [https://doi.org/10.5194/esurf-](https://doi.org/10.5194/esurf-2-1-2014)
1022 [2-1-2014](https://doi.org/10.5194/esurf-2-1-2014), 2014.

1023 Shea, T. and van Wyk de Vries, B.: Structural analysis and analogue modeling of the kinematics and dynamics of
1024 rockslide avalanches, *Geosphere*, 4, 657–686, <https://doi.org/10.1130/GES00131.1>, 2008.

1025 Sklar, L. S. and Dietrich, W. E.: Sediment and rock strength controls on river incision into bedrock, *Geology*, 29,
1026 1087–1090, [https://doi.org/10.1130/0091-7613\(2001\)029<1087:SARSCO>2.0.CO;2](https://doi.org/10.1130/0091-7613(2001)029<1087:SARSCO>2.0.CO;2), 2001.

1027 Strahler, A. N.: Hypsometric (area-altitude) analysis of erosional topography, *Bull. Geol. Soc. Am.*, 63, 1117–1142,
1028 <https://doi.org/10.1128/AAC.03728-14>, 1952.

1029 Sweeney, K. E. and Roering, J. J.: Rapid fluvial incision of a late Holocene lava flow: Insights from LiDAR, alluvial
1030 stratigraphy, and numerical modeling, *Bull. Geol. Soc. Am.*, 129, 500–512, <https://doi.org/10.1130/B31537.1>, 2017.

1031 Talling, P. J., Stewart, M. D., Stark, C. P., Gupta, S., and Vincent, S. J.: Regular spacing of drainage outlets from
1032 linear fault blocks, *Basin Res.*, 9, 275–302, <https://doi.org/10.1046/j.1365-2117.1997.00048.x>, 1997.

1033 Thouret, J. C., Oehler, J. F., Gupta, A., Solikhin, A., and Procter, J. N.: Erosion and aggradation on persistently
1034 active volcanoes—a case study from Semeru Volcano, Indonesia, *Bull. Volcanol.*, 76,
1035 <https://doi.org/10.1007/s00445-014-0857-z>, 2014.

1036 Ui, T. and Glicken, H.: Internal structural variations in a debris-avalanche deposit from ancestral Mount Shasta,
1037 California, USA, *Bull. Volcanol.*, 48, 189–194, <https://doi.org/10.1007/BF01087673>, 1986.

1038 van Wees, R. M. J., Tournigand, P.-Y., O'Hara, D., Grosse, P., Kereszturi, G., Campforts, B., Lahitte, P., and
1039 Kervyn, M.: The role of erosion in the morphometry of composite volcanoes, in: EGU General Assembly

Deleted: Quidelleur, X., Ricci, J., Lahitte, P.,

1041 Conference Abstracts, EGU21-14500, 2021.

1042 Wells, S. G., Dohrenwend, J. C., McFadden, L. D., Turrin, B. D., and Mahrer, K. D.: Late Cenozoic landscape
1043 evolution on lava flow surfaces of the Cima volcanic field, Mojave Desert, California., *Geol. Soc. Am. Bull.*, 96,
1044 1518–1529, [https://doi.org/10.1130/0016-7606\(1985\)96<1518:LCLEOL>2.0.CO;2](https://doi.org/10.1130/0016-7606(1985)96<1518:LCLEOL>2.0.CO;2), 1985.

1045 Whipple, K. X., DiBiase, R. A., Ouimet, W. B., and Forte, A. M.: Preservation or piracy: Diagnosing low-relief,
1046 high-elevation surface formation mechanisms, *Geology*, 45, 91–94, <https://doi.org/10.1130/G32501Y.1>, 2016.

1047 Wicks, C. W., Dzurisin, D., Ingebritsen, S., Thatcher, W., Lu, Z., and Iverson, J.: Magmatic activity beneath the
1048 quiescent Three Sisters volcanic center, central Oregon Cascade Range, USA, *Geophys. Res. Lett.*, 29, 26-1-26–4,
1049 <https://doi.org/10.1029/2001GL014205>, 2002.

1050 Willett, S. D., Slingerland, R., and Hovius, N.: Uplift, shortening, and steady state topography in active mountain
1051 belts, *Am. J. Sci.*, 301, 455–485, <https://doi.org/10.2475/ajs.301.4-5.455>, 2001.

1052 Willett, S. D., McCoy, S. W., Perron, T. J., Goren, L., and Chen, C. Y.: Dynamic reorganization of River Basins,
1053 *Science (80-.)*, 343, <https://doi.org/10.1126/science.1248765>, 2014.

1054 Yang, R., Willett, S. D., and Goren, L.: In situ low-relief landscape formation as a result of river network disruption,
1055 *Nature*, 520, 526–529, <https://doi.org/10.1038/nature14354>, 2015.

1056 Zernitz, E. R.: Drainage Patterns and Their Significance, *J. Geol.*, 40, 498–521, <https://doi.org/10.1086/623976>,
1057 1932.

1058

Page 4: [1] Deleted **Daniel** **3/8/2024 7:25:00 PM**

Although automated algorithms exist to generate boundaries (e.g., Bohnenstiehl et al., 2012; Euillades et al., 2013), these often create conservative limits around the edifice that ignore lower flanks and volcano-sedimentary aprons (e.g., O'Hara et al., 2020).

Page 4: [2] Deleted **Daniel** **3/8/2024 7:25:00 PM**

None of the chosen volcanoes have closed summit craters, recognizable collapse scars, or any other irregular surface that required special preprocessing; we thus use the entire edifice topography for our analysis.

Page 4: [3] Deleted **Daniel** **3/8/2024 7:25:00 PM**

a: Map of Ungaran volcano (Indonesia), colored lines defined in legend.

Page 4: [4] Deleted **Daniel** **3/8/2024 7:25:00 PM**

Black circles are basins used in power-law analysis, black dots are excluded basins; blue-dashed line is drainage area threshold (A_T ; 0.5 km^2) for channelization.

Page 4: [5] Deleted **Daniel** **3/8/2024 7:25:00 PM**

Gray line represents cross-basin direction perpendicular to the Euclidean basin length.

Page 4: [6] Deleted **Daniel** **3/8/2024 7:25:00 PM**

Black line is relief along flowpath, blue line is cross-valley width.

Page 10: [7] Formatted **Daniel** **3/8/2024 7:25:00 PM**

Font: Not Bold

Page 10: [7] Formatted **Daniel** **3/8/2024 7:25:00 PM**

Font: Not Bold

Page 10: [8] Formatted **Daniel** **3/8/2024 7:25:00 PM**

Font: Not Bold

Page 10: [8] Formatted **Daniel** **3/8/2024 7:25:00 PM**

Font: Not Bold

Page 10: [9] Formatted **Daniel** **3/8/2024 7:25:00 PM**

Font: Not Bold

Page 10: [9] Formatted **Daniel** **3/8/2024 7:25:00 PM**

Font: Not Bold

Page 10: [10] Deleted **Daniel** **3/8/2024 7:25:00 PM**

volcanic edifices

Page 10: [10] Deleted Daniel 3/8/2024 7:25:00 PM

volcanic edifices

Page 10: [11] Deleted Daniel 3/8/2024 7:25:00 PM

volcanic edifice

Page 10: [11] Deleted Daniel 3/8/2024 7:25:00 PM

volcanic edifice

Page 10: [11] Deleted Daniel 3/8/2024 7:25:00 PM

volcanic edifice

Page 10: [11] Deleted Daniel 3/8/2024 7:25:00 PM

volcanic edifice

Page 10: [11] Deleted Daniel 3/8/2024 7:25:00 PM

volcanic edifice

Page 10: [11] Deleted Daniel 3/8/2024 7:25:00 PM

volcanic edifice

Page 16: [12] Formatted Daniel 3/8/2024 7:25:00 PM

Font: Not Bold

Page 16: [12] Formatted Daniel 3/8/2024 7:25:00 PM

Font: Not Bold

Page 16: [12] Formatted Daniel 3/8/2024 7:25:00 PM

Font: Not Bold

Page 16: [13] Formatted Daniel 3/8/2024 7:25:00 PM

Font: Not Bold

Page 16: [13] Formatted Daniel 3/8/2024 7:25:00 PM

Font: Not Bold

Page 16: [14] Formatted Daniel 3/8/2024 7:25:00 PM

Font: Not Bold

Page 16: [14] Formatted **Daniel** **3/8/2024 7:25:00 PM**

Font: Not Bold

Page 16: [14] Formatted **Daniel** **3/8/2024 7:25:00 PM**

Font: Not Bold

Page 16: [15] Deleted **Daniel** **3/8/2024 7:25:00 PM**

Our analysis indicates that basins with drainage areas greater than 10^5 m² are well-fit by a power-law regression (Figs. 2b, 9a, c), whereas basins smaller than 10^5 m² have steeper trends between basin area and length, and are likely non-fluvial within the bounds of the edifice.

Page 16: [15] Deleted **Daniel** **3/8/2024 7:25:00 PM**

Our analysis indicates that basins with drainage areas greater than 10^5 m² are well-fit by a power-law regression (Figs. 2b, 9a, c), whereas basins smaller than 10^5 m² have steeper trends between basin area and length, and are likely non-fluvial within the bounds of the edifice.

Page 16: [15] Deleted **Daniel** **3/8/2024 7:25:00 PM**

Our analysis indicates that basins with drainage areas greater than 10^5 m² are well-fit by a power-law regression (Figs. 2b, 9a, c), whereas basins smaller than 10^5 m² have steeper trends between basin area and length, and are likely non-fluvial within the bounds of the edifice.

Page 16: [15] Deleted **Daniel** **3/8/2024 7:25:00 PM**

Our analysis indicates that basins with drainage areas greater than 10^5 m² are well-fit by a power-law regression (Figs. 2b, 9a, c), whereas basins smaller than 10^5 m² have steeper trends between basin area and length, and are likely non-fluvial within the bounds of the edifice.

Page 18: [16] Formatted **Daniel** **3/8/2024 7:25:00 PM**

Font: Not Bold

Page 18: [16] Formatted **Daniel** **3/8/2024 7:25:00 PM**

Font: Not Bold